Global and Planetary Change 108 (2013) 85–99

Contents lists available at SciVerse ScienceDirect

Global and Planetary Change

journal homepage: www.elsevier.com/locate/gloplacha

# Response of evapotranspiration and water availability to changing climate and land cover on the Mongolian Plateau during the 21st century

Yaling Liu [a,*], Qianlai Zhuang [a,b], Min Chen [a], Zhihua Pan [c,d], Nadja Tchebakova [e], Andrei Sokolov [f], David Kicklighter [g], Jerry Melillo [g], Andrey Sirin [h], Guangsheng Zhou [i], Yujie He [a], Jiquan Chen [j], Laura Bowling [b], Diego Miralles [k], Elena Parfenova [e]

[a] Department of Earth, Atmospheric and Planetary Sciences, Purdue University, West Lafayette, IN 47907, USA
[b] Department of Agronomy, Purdue University, West Lafayette, IN 47907, USA
[c] College of Resources and Environmental Sciences, China Agricultural University, Beijing 100193, China
[d] Key Ecology and Environment Experimental Station for Field Scientific Observation in Huhhot, Ministry of Agriculture, Inner Mongolia 011705, China
[e] V N Sukachev Institute of Forest, Siberian Branch of the Russian Academy of Sciences, Academgorodok, Krasnoyarsk 660036, Russia
[f] Department of Earth, Atmospheric, and Planetary Sciences, Massachusetts Institute of Technology, Cambridge, MA 02139, USA
[g] The Ecosystems Center, Marine Biological Laboratory, Woods Hole, MA 02543, USA
[h] Laboratory of Peatland Forestry and Amelioration, Institute of Forest Science, Russian Academy of Sciences, Uspenskoye, Moscow Oblast 143030, Russia
[i] State Key Laboratory of Vegetation and Environmental change, Institute of Botany, The Chinese Academy of Sciences, Beijing 100093, China
[j] Department of Environmental Sciences, University of Toledo, Toledo, OH 43606, USA
[k] School of Geographical Sciences, University of Bristol, Bristol, UK

ARTICLE INFO

*Article history:*
Received 17 September 2012
Accepted 13 June 2013
Available online 21 June 2013

*Keywords:*
Evapotranspiration
Mongolian Plateau
Terrestrial Ecosystem Model
MODIS
Climate change
Land cover change

ABSTRACT

Adequate quantification of evapotranspiration (ET) is crucial to assess how climate change and land cover change (LCC) interact with the hydrological cycle of terrestrial ecosystems. The Mongolian Plateau plays a unique role in the global climate system due to its ecological vulnerability, high sensitivity to climate change and disturbances, and limited water resources. Here, we used a version of the Terrestrial Ecosystem Model that has been modified to use Penman–Monteith (PM) based algorithms to calculate ET. Comparison of site-level ET estimates from the modified model with ET measured at eddy covariance (EC) sites showed better agreement than ET estimates from the MODIS ET product, which overestimates ET during the winter months. The modified model was then used to simulate ET during the 21st century under six climate change scenarios by excluding/including climate-induced LCC. We found that regional annual ET varies from 188 to 286 mm $yr^{-1}$ across all scenarios, and that it increases between 0.11 mm $yr^{-2}$ and 0.55 mm $yr^{-2}$ during the 21st century. A spatial gradient of ET that increases from the southwest to the northeast is consistent in all scenarios. Regional ET in grasslands, boreal forests and semi-desert/deserts ranges from 242 to 374 mm $yr^{-1}$, 213 to 278 mm $yr^{-1}$ and 100 to 199 mm $yr^{-1}$, respectively; and the degree of the ET increase follows the order of grassland, semi-desert/desert, and boreal forest. Across the plateau, climate-induced LCC does not lead to a substantial change (<5%) in ET relative to a static land cover, suggesting that climate change is more important than LCC in determining regional ET. Furthermore, the differences between precipitation and ET suggest that the available water for human use (water availability) on the plateau will not change significantly during the 21st century. However, more water is available and less area is threatened by water shortage in the Business-As-Usual emission scenarios relative to level-one stabilization emission scenarios.



## 1. Introduction

Evapotranspiration (ET) is an essential component of the hydrologic cycle, and is central to earth system science because it governs interactions (e.g., energy exchange and biogeochemical cycling) between the atmosphere and terrestrial ecosystems (Betts et al., 1996; Mu et al., 2007; Weiß and Menzel, 2008; Dolman and De Jeu, 2010; Wang et al., 2010; Mu et al., 2011; Sun et al., 2011a, 2011b; Katul et al., 2012; Wang and Dickinson, 2012). ET returns more than 60% of annual land precipitation back to the atmosphere (Shiklomanov et al., 1983; L'vovich et al., 1990; Oki and Kanae, 2006; Miralles et al., 2011a), and thereby constrains water availability over the continents. Future trends of ET may lead to an overall intensification or weakening of the water cycle, with implications for the recycling of precipitation and generation

* Corresponding author at: 550 Stadium Mall Drive, West Lafayette, IN 47907-2051, USA. Tel.: +1 765 494 2434.
*E-mail address:* liu516@purdue.edu (Y. Liu).

0921-8181/$ – see front matter © 2013 Elsevier B.V. All rights reserved.
http://dx.doi.org/10.1016/j.gloplacha.2013.06.008

of runoff (Shukla et al., 1990; Lean et al., 1995). With a growing scientific consensus about global warming (Hansen et al., 2005; Barnett et al., 2005; IPCC, 2007), there is an increasing concern about how climatic change will impact the water supply, especially in arid and semi-arid regions (Vorosmarty et al., 2000; Peterson et al., 2002; Serreze and Barry, 2005; Peterson et al., 2006; IPCC, Intergovernmental Panel on Climate Change, 2007; Bates et al., 2008). These issues are directly relevant to human society and play an important role in the policy-making process related to water management.

Quantitative predictions of regional water balances, management of water resources, irrigation scheduling, or climate and weather prediction, all require the accurate quantification of ET. (Valiantzas, 2006; Cleugh et al., 2007; Jiang et al., 2009; Wang et al., 2010; Mu et al., 2011; Wang and Dickinson, 2012). Simulations from models which have been calibrated and parameterized with measured data (e.g., measurements at EC towers), and satellite-based estimates can then be used for continuous predictions over time and space (Jung et al., 2010; Xiao et al., 2012).

The Mongolian Plateau offers an interesting opportunity to study the state-of-the-art ET dynamics. It is located in a farming–pastoral ecotone adjoining the Gobi desert in the south and the Altai-Sayan Mountains in the north, and is dominated by arid and semi-arid climate (He et al., 2009; Lu et al., 2009; Liu et al., 2011). The plateau covers vast arid and semi-arid area, and is expected to experience earlier and more drastic climate changes (e.g., surface air temperature) compared with lower latitude regions (IPCC (Intergovernmental Panel on Climate Change), 2001; Zhuang et al., 2004; Lu et al., 2009). Additionally, the high vulnerability of the ecosystem makes it especially sensitive to climate change and disturbances (Sun et al., 2002; Sankey et al., 2006; Dulamsuren et al., 2009; Lu et al., 2009; Chen et al., 2012). The plateau is therefore considered to play a critical role in the global climate system (Galloway and Melillo, 1998; Li et al., 2008; Lu et al., 2009). As in other arid and semi-arid regions – where water loss from ET can account for >95% of the annual precipitation (Kurc and Small, 2004; Huxman et al., 2005; Lu et al., 2011; Sun et al., 2011b; Wang et al., 2011; Katul et al., 2012) – ET is crucial in controlling the hydrology, climate and ecology in the plateau. As the climate and land cover of the plateau have been projected to change during the 21st century (Lu et al., 2009; Tchebakova et al., 2009; Groisman et al., 2010), the regional ET could change significantly.

Investigation of future trends in ET under changing climate and climate-induced LCC on the plateau can provide insights into how climate policies might influence future water supplies, and contribute to the understanding of future hydrological, ecological and societal changes in this region and their feedbacks to the global climate system. To date, there is a lack of studies on the quantification of ET and water availability under changing climate and land cover on the Mongolian Plateau. This study is a pioneer effort toward filling that knowledge gap. The first objective of this study is to improve the ET algorithms of a process-based biogeochemistry model — the Terrestrial Ecosystem Model (TEM; Zhuang et al., 2003, 2010). Then, we aim to validate and apply the improved model to examine how ET will respond to the changes of climate and land cover over the plateau during the 21st century. The implications of the results for the water availability in the region will be discussed in detail.

## 2. Methods

The Terrestrial Ecosystem Model (TEM) is a process-based biogeochemistry model using spatially referenced data of climate, soils, land cover, and elevation to simulate C, N, and water fluxes and pool sizes of the terrestrial biosphere (e.g., Raich et al., 1991; McGuire et al., 1992; Zhuang et al., 2001, 2002, 2003, 2004). In this study, we modified TEM version 5.0 (Zhuang et al., 2003, 2010) to incorporate algorithms based on the Penman–Monteith (PM) equation (Monteith, 1965; Allen et al., 1998) to estimate ET. These modifications allowed better consideration of interactions between terrestrial energy and water budgets when estimating ET with TEM. To evaluate these model improvements, site-level ET estimates of the TEM, with and without modifications of the ET algorithms, were compared against ET measurements from two eddy covariance sites on the Mongolian Plateau. In addition, regional ET estimates by TEM, with and without modifications of the ET algorithms, were compared to the regional estimates from the three recent studies (Miralles et al., 2011a,b; Mu et al., 2011; Vinukollu et al., 2011). The modified TEM was then used with six climate change scenarios and two land cover scenarios to examine how ET might respond to changes of climate and land cover over the plateau during the 21st century.

### 2.1. Modeling algorithms

In the previous version of monthly time-step TEM (Zhuang et al., 2003, 2010), the ET algorithms (hereafter referred to as AL1) are based on both the atmospheric demand for water vapor and the ability of the land surface to supply such water vapor (Vörösmarty et al., 1998). In the previous TEM, the atmospheric demand for water vapor is determined from potential evapotranspiration (PET, mm $mon^{-1}$), which is estimated via the Jensen and Haise (1963) formulation:

$$PET = [(0.014 \times (1.8 \times T + 32) - 0.37)] \times R_s \times 0.016742 \times MD \quad (1)$$

where T is the monthly average air temperature (°C), $R_s$ is the mean monthly short-wave radiation at the top of the canopy (Cal $cm^{-2}$ $d^{-1}$) calculated in TEM using latitude, date and cloudiness (Pan et al., 1996), and MD is the number of days per month. This PET algorithm does not consider the effects of net outgoing long-wave radiation from the land surface, ground heat flux, and the aerodynamic aspects of ET on the atmospheric demand for water vapor. PET calculated in Eq. (1) tends to be underestimated in the spring and overestimated in the summer, as the sensitivity of PET to T is larger, and the sensitivity to $R_s$ is lower than in nature (Feddes and Lenselink, 1994). Biases in the calculation of PET will then be propagated to the ET estimates.

ET is then derived from PET in conjunction with a water balance model (WBM), where the ability of the land surface to supply water for ET depends on the amount of soil moisture (SM), rainfall and snowmelt (Vörösmarty et al., 1998). In the WBM, direct surface runoff is not separated from total runoff from a grid cell, which is assumed to go through soils and contribute to neighboring stream networks. If the sum of monthly rainfall and snowmelt is greater or equal to monthly PET, then ET is assumed to equal PET. If SM reaches field capacity under these conditions, then any additional water is assumed to be runoff to neighboring river networks. If the sum of monthly rainfall and snowmelt is less than the monthly PET, then no runoff is assumed to occur and ET is calculated by subtracting the change in SM during the month from the sum of monthly rainfall and snowmelt. A unitless soil drying function is used to determine the change in SM within a month based on relative soil wetness, PET, rainfall and snowmelt.

To improve ET estimates within the monthly time-step TEM, we introduced new ET algorithms (hereafter referred to as AL2), based on the PM algorithm as applied by Mu et al (2007, 2011) that explicitly incorporates both physiological and aerodynamic constraints (Monteith, 1965; Allen et al., 1998). In these new AL2 algorithms, we calculated ET (mm $mon^{-1}$) by estimating transpiration of the vegetation canopy ($T_c$, mm $mon^{-1}$) separately from evaporation from the soil surface ($E_{soil}$, mm $mon^{-1}$):

$$ET = T_c + E_{soil} \quad (2a)$$

$$T_c = \frac{sA_c + \rho c_p (VPD)/r_a}{\lambda(s + \gamma(1 + r_s/r_a))} \times secs2day \times MD \quad (2b)$$

$$E_{soil_{pot}} = \frac{sA_{soil} + \rho c_p (VPD)/r_{as}}{\lambda(s + \gamma(1 + r_{tot}/r_{as}))} \times secs2day \times MD \quad (2c)$$

$$E_{soil} = E_{soil_{pot}} \times f_{SM} \quad (2d)$$

$$f_{SM} = RH^{VPD/\beta} \quad (2e)$$

where $A_c$ (W $m^{-2}$) is the available energy in the vegetation canopy, $A_{soil}$ (W $m^{-2}$) is the available energy in the soil, s is the slope of the saturation vapor pressure curve (Pa $K^{-1}$) and is a function of air temperature, $\rho$ (kg $m^{-3}$) is the air density, $c_p$ (J $kg^{-1}$ $K^{-1}$) is the specific heat capacity of air, VPD (Pa) is the vapor pressure deficit (i.e., saturated air vapor pressure minus actual air vapor pressure), $r_a$ (s $m^{-1}$) is the aerodynamic resistance, $r_s$ (s $m^{-1}$) is the surface resistance to transpiration from the plant canopy, $r_{as}$ is the aerodynamic resistance at the soil surface, $r_{tot}$ is the sum of $r_{as}$ and surface resistance to evaporation, $\lambda$ (J $kg^{-1}$) is the latent heat of vaporization, $\rho$ (kg $m^{-3}$) is the air density, $\gamma$ (Pa $K^{-1}$) is the psychometric constant, secs2day (s $day^{-1}$) is the number of seconds in a day, $E_{soil\_pot}$ is the potential evaporation from soils, $f_{SM}$ is a proxy of soil water deficit used to constrain soil evaporation, RH is relative humidity, and $\beta$ is the relative sensitivity of RH to VPD (Fisher et al., 2008).

As described by Mu et al. (2011), the available energy in the vegetation canopy ($A_c$) to support transpiration is determined by multiplying the net radiation flux at the surface ($R_n$, W $m^{-2}$) by the fraction of ground covered by vegetation ($F_c$), whereas the available energy in the soil depends on $R_n$ multiplied by the fraction of ground not covered by vegetation ($1 - F_c$) minus the sensible heat exchange from the surface into the soil (G, W $m^{-2}$). $R_n$ is the balance of incoming and outgoing shortwave and longwave radiation and is calculated from the incoming shortwave radiation ($R_s$), albedo, and air temperature as described by Cleugh et al. (2007). Mean monthly values for albedo and air temperature are used when calculating $R_n$.

Based on the protocols of Mu et al. (2007), and the relationships among the Fraction of Absorbed Photosynthetically Active Radiation (FPAR), leaf area index (LAI) and enhanced vegetation index (Turner et al., 2003; Heinsch et al., 2006; Hu et al., 2007; Chen et al., 2009), $F_c$ is calculated as:

$$F_c = \frac{\exp(-LAI_{min} \times k) - \exp(-LAI \times k)}{\exp(-LAI_{min} \times k) - \exp(-LAI_{max} \times k)} \quad (3)$$

where $LAI_{min}$ and $LAI_{max}$ are the minimum and maximum LAI in a year, respectively, and k is the canopy light extinction coefficient and assumed to be 0.5 (Running and Coughlan, 1988). Monthly LAI is estimated by TEM as follows:

$$LAI = SLA \times ALLEAF \times LEAF \quad (4)$$

where SLA is the specific leaf area ($m^2$/gC) (Pierce et al., 1994; Garnier et al., 1997; Poorter and Evans, 1998; White et al., 2000; Milner et al., 2003), ALLEAF is the maximum leaf biomass (g C $m^{-2}$), and LEAF is a phenology term that represents the relative amount of leaf biomass in a specific month to ALLEAF and is estimated by TEM (Zhuang et al., 2002).

G is estimated based on monthly air temperature (Allen et al., 1998):

$$G = 1.6198(T_i - T_{i-1}) \quad (5)$$

where $T_i$ is the mean air temperature of month i (°C) and $T_{i-1}$ is that of the previous month (°C).

Soil evaporation is calculated from potential soil evaporation ($E_{soil\_pot}$) and is constrained by a proxy of soil water deficit $f_{SM}$. The estimate of $f_{SM}$ is based on the complementary relationship of land-atmosphere interactions from VPD and RH, where it is assumed that SM has a strong link with the adjacent atmospheric moisture (Bouchet, 1963; Mu et al., 2007; Fisher et al., 2008).

The detailed methods for calculating the $r_s$ and $r_a$ of plant transpiration, the $r_{tot}$ and $r_{as}$ of soil surface evaporation are documented in Mu et al. (2007, 2011). $r_s$ in Eq. (2b), is calculated from canopy conductance $C_c$ (the inverse of $r_s$), which is based on the mean potential stomatal conductance per unit leaf area ($C_L$), LAI, VPD, and air temperature (Mu et al., 2007). The effects of environmental factors such as VPD and air temperature on the stomatal resistance (converted to $r_s$ using 1/LAI as a scalar), $r_{tot}$ and $r_{as}$ have been taken into account in this study, and the effects of air temperature on $r_a$ have also been considered. In addition, although the effects of SM on $r_{tot}$ and stomatal resistance have not been directly incorporated in their calculation, $f_{SM}$ has been applied as a SM constraint on soil evaporation, and further control is represented as ET estimates are constrained by the soil water balance in TEM. Some other ET methodologies like the one by Miralles et al. (2011a, 2011b) explicitly use SM and vegetation water content observations to estimate evaporative stress. Additionally, many previous studies consider other environmental factors for calculating resistances than those considered in this study, such as net radiation, photosynthetically active radiation flux (PAR), ambient $CO_2$ concentrations and wind (Jarvis, 1976; Sellers et al., 1986; Ball 1987; Dolman et al., 1991; Xu et al., 1994; Wright et al., 1995; ASCE, American Society of Civil Engineers, 1996; Dickinson et al., 1998; Mueller et al., 2011). Consideration of these factors allows the estimation of resistance to capture more specific effects of biophysical properties on ET, but provide limited benefits to our monthly time-step simulations and also introduce additional uncertainties. Given that $r_a$ and $r_{as}$ are very sensitive to wind speed variation (ASCE, American Society of Civil Engineers, 1996; Liu et al., 2006; Zhang et al., 2007; Bonan, 2008), an average monthly wind will smooth most of the "noise" and short-term variation so that it is likely to fail to capture the effects of wind on $r_a$ and $r_{as}$. Moreover, the current unavailability of wind speed data in the Integrated Global System Model (ISGM) climate scenarios data (driving data of this study) makes it unfeasible to incorporate wind into the parameterizations of $r_a$ and $r_{as}$. Similarly, the diurnal cycle of stomatal resistance responds to the diurnal variability of $R_n$ and PAR (Landsberg and Gower, 1996), but most of this response would be lost using averaged monthly aggregates.

Finally, after calculating ET with the new AL2 algorithms, the ET estimates were then constrained by the available water in soils as determined by water balance in TEM. Thus, ET estimated using either the AL1 or AL2 algorithms (hereafter referred to as AL1-ET and AL2-ET, respectively) is constrained by the soil water balance, but the AL2 now considers more aspects of the concurrent energy balance and more effects of environmental and biophysical factors on ET than the AL1 of the previous TEM.

### 2.2. Model parameterization

As described above, here we modified TEM version 5.0 (Zhuang et al., 2003, 2010) by adapting algorithms developed by Mu et al. (2007, 2011) based on the PM equation (Monteith, 1965; Allen et al., 1998) for estimating ET by TEM. Many parameters involved in the new AL2 algorithms were defined from literature values (e.g., Running and Coughlan, 1988; Shuttleworth, 1992; ASCE, American Society of Civil Engineers, 1996; Milner et al., 2003; Cleugh et al., 2007; Mu et al., 2007, 2011), while other parameters such as the relative sensitivity of RH to VPD ($\beta$), specific leaf area (SLA), and mean potential stomatal conductance per unit leaf area ($C_L$) for grasslands and boreal forests were adjusted within the referenced range until model values were closest to field-based measured ET. The major parameters that were introduced into or adjusted in this study are listed in Table 1.

For albedo, we used MODIS albedo (MCD43C3) of year 2005 for the region to determine the mean monthly albedo of each land cover type (Schaaf et al., 2002; Jin et al., 2003a, 2003b; Salomon et al., 2006;

**Table 1**
Values of major parameters attained through parameterization or estimation from reference. SD: semidesert/desert; WT: wet tundra; BF: boreal forest; TF: temperate forests; GR: grasslands.

| Parameter | SD | WT | BF | TF | GR | References |
|---|---|---|---|---|---|---|
| β (hpa) | 2.0 | 2.0 | 1.50 | 1.5 | 2.1 | Mu. et al. (2007, 2011) and Fisher et al. (2008) |
| SLA ($m^2$/gC) | 0.05 | 0.05 | 0.02 | 0.025 | 0.05 | Milner et al. (2003), White et al. (2000), Poorter and Evans (1998) and Garnier et al. (1997) |
| $C_L$ (m/s) | 0.005 | 0.004 | 0.0032 | 0.003 | 0.005 | Mu. et al. (2007, 2011) and Cleugh et al. (2007) |

http://www-modis.bu.edu/brdf/userguide/cmgnbar.html), which was assumed to remain unchanged during 1971–2100 due to unavailability of time series albedo data. Then the monthly albedo of each land cover was used as land cover-specific parameters to estimate monthly $R_n$.

### 2.3. Data

Overall, TEM needs input data on air temperature, precipitation, cloudiness, vapor pressure, atmospheric $CO_2$ concentrations, land cover type, albedo, elevation, and soil texture to estimate ET. As indicated earlier, TEM can use cloudiness data to estimate incoming shortwave radiation. Soil texture and elevation vary spatially over the study regions and are assumed to remain static throughout 1971–2100, whereas other inputs vary over time and space. In this study, we conducted our simulations at a spatial resolution of 0.5° latitude × 0.5° longitude resolution so that all spatially-explicit input data sets were reorganized to this resolution.

#### 2.3.1. Historical data

Data on soil texture, elevation, and historical climate and atmospheric $CO_2$ concentrations from 1971 to 2000 were collected from several sources. The soil texture data were from the Food and Agriculture Organization/Civil Service Reform Committee (FAO/CSRC) digitization of the FAO–UNESCO (1971) soil map (Zobler, 1986). Elevation data were from the Shuttle Radar Topography Mission (Farr, 2007). Gridded historical data on monthly air temperature, precipitation, cloudiness, and vapor pressure were obtained from the Climate Research Unit (CRU) of the University of East Anglia. Annual global atmospheric $CO_2$ concentration data for the historical period were acquired from atmospheric observations (Keeling and Whorf, 2005).

#### 2.3.2. Future scenarios data

Modeling estimates of changes in air temperature, precipitation, cloudiness, vapor pressure, and atmospheric $CO_2$ concentrations associated with six climate scenarios (X901M, X902L, X903H, X904M, X905L, and X906H; Sokolov et al., 2005; Zhu et al., 2011; Jiang et al., 2012) generated by the IGSM of the Massachusetts Institute of Technology (MIT) (Sokolov et al., 2005) were used for future projections over the 21st century. The X901M, X902L, and X903H scenarios represent Business-As-Usual (BAU) emission scenarios with a median climate response, a low climate response, and a high climate response, respectively. The X904M, X905L, and X906H scenarios represent level-one stabilization emission (450 ppm $CO_2$) scenarios with a median climate response, a low climate response, and a high climate response, respectively. The largest increases in air temperature and precipitation occur in the X903H scenario and the smallest increases occur in the X905L scenario on the plateau (Fig. 1).

Each of the six climate scenarios was used to drive a biogeography model, Siberian BioClimatic Model (SiBCliM, Tchebakova et al., 2009, 2011), to simulate land cover distribution for the years 2000, 2025, 2050, 2075 and 2100. Other than climate change, the SiBCliM simulations did not consider the influence of any anthropogenic activities on land cover distribution. Land cover simulations of 2000 are used to represent a static land cover throughout 1971–2100 (referred to as VEG1). To examine the effects of climate-induced LCC, the simulated land cover was used to develop a time series of annual land cover over five time periods from 2001 to 2100. The SiBCliM results for 2000, 2025, 2050, 2075 and 2100 were used to describe land cover during 2000–2024, 2025–2049, 2050–2074, 2075–2099, and 2100,

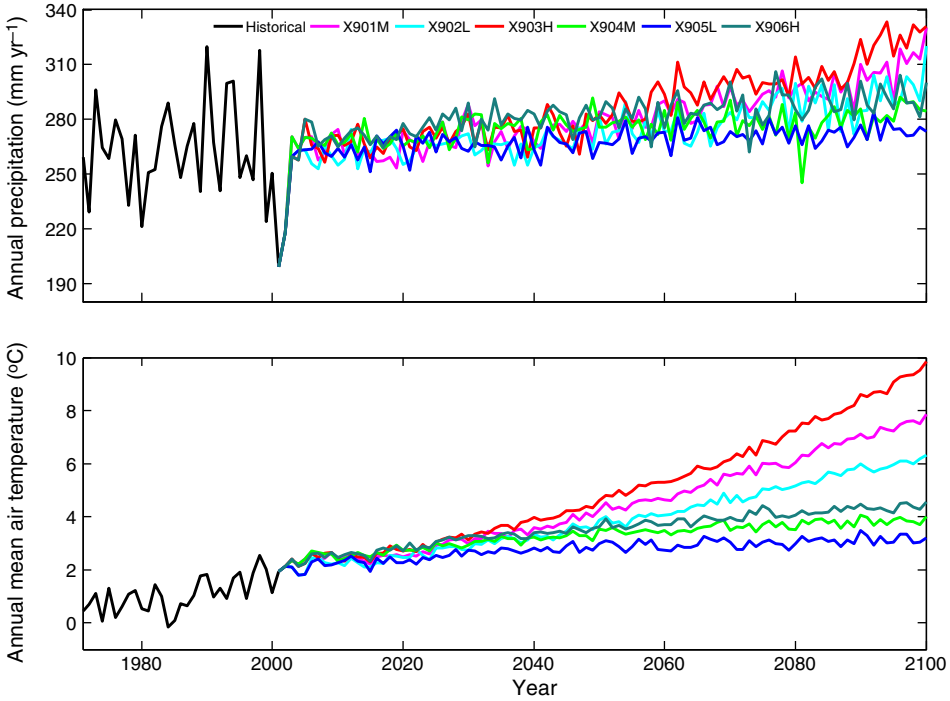


**Fig. 1.** Climate variation of the Mongolia plateau during the period of 1971–2100 in X901M, X902L, X903H, X904M, X905L, and X906H: (a) annual precipitation, and (b) annual mean air temperature.

respectively (referred to as VEG2). The annual land cover distribution in VEG2 is assumed to remain unchanged from year to year throughout each period but varies among the five periods (Fig. 2).

*2.3.3. Data for model evaluation*

Data were obtained to evaluate the performance of the modifications to TEM at both the site and regional levels. In addition to latent heat fluxes, EC data of air temperature, precipitation, RH, and incoming shortwave radiation were collected from two Mongolian sites (http://www.asianflux.com) to allow the development of site level ET estimates by TEM: a larch forest site at Southern Khentei Taiga (SKT) and a grassland site at Kherlenbayan Ulaan (KBU). The half-hourly data at SKT and KBU are available from 2003 to 2006, and 2003 to 2009, respectively. An Artificial Neural Network method (Papale and Valentini, 2003) was used to fill any gaps in the data caused by system failure or data rejection. We then averaged half-hourly air temperature, RH, latent heat flux, and solar radiation, and summed the half-hourly precipitation to get monthly values.

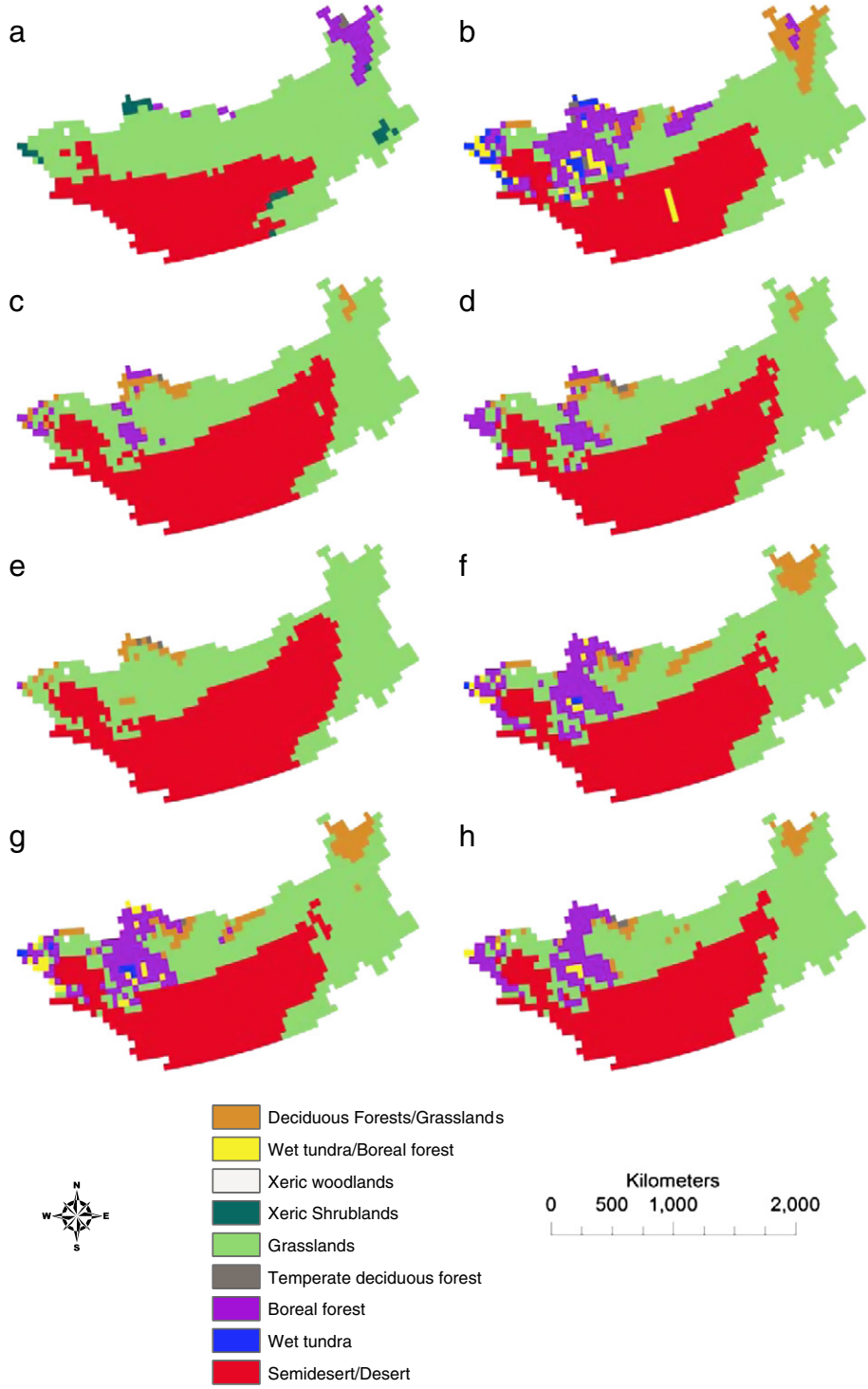


**Fig. 2.** Land cover of Mongolia plateau from (a) MODIS land cover data of 2001, and from SibClim simulation of (b) 2000, (c) 2100 in X901M, (d) 2100 in X902L, (e) 2100 in X903H, (f) 2100 in X904M, (g) 2100 in X905L, and (h) 2100 in X906H.

Monthly ET estimates from MODIS (referred to as MODIS-ET, Mu et al., 2011) and from GLEAM (Global Land-surface Evaporation: the Amsterdam Methodology — Miralles et al., 2011a, b) were also collected and compared to site-level ET estimates by TEM. Although AL2-ET and MODIS-ET estimates are both based on PM framework, they are different in LAI acquisition, calculation of $F_c$ and G, parameterization of $C_L$, β and SLA, forcing data, and whether is constrained by available soil water.

For evaluation of spatial and temporal patterns of ET estimated by TEM across the plateau, AL2-ET results were also compared to gridded estimates selected out of global results by Vinukollu et al. (2011) in addition to MODIS-ET and GLEAM for the time period 2000 to 2008. Vinukollu et al. (2011) also used a PM based approach extended by Mu et al. (2007) to estimate ET (known as PM-Mu ET) whereas GLEAM is based on a Priestley–Taylor approach with an evaporative constraint base on satellite-derived soil moisture and vegetation water content (Miralles et al., 2011a,b). For these regional evaluations, TEM was driven with monthly air temperature, precipitation, dew point temperature (used to derive vapor pressure), and cloudiness data over the 2000–2008 time period obtained from the European Centre for Medium-Range Weather Forecasts (ECMWF). MODIS land cover data of 2001 were used (MCD12C1), with an assumption that the land cover of the plateau during 2000–2008 was the same as 2001.

### 2.4. Regional simulations

ET simulations were conducted for both static and changing land cover conditions. The model was first run to equilibrium using the long-term averaged historical monthly climate data from 1971 to 2000, and was then spun up for 120 years to develop initial conditions for TEM at the beginning of the 21st century for the plateau. Then, we conducted twelve simulations using the AL2 algorithms to examine the effects of future climate change and LCC on ET. To examine the effects of climate change alone on ET, we conducted six simulations using the VEG1 land cover, historical climate from 1971 to 2000, and each of the six climate scenarios from 2001 to 2100. To examine the effects of both climate change and climate-induced LCC on ET during the 21st century, we conducted six simulations using the VEG2 land cover, historical climate from 1971 to 2000, and each of the six climate scenarios from 2001 to 2100. Differences in ET between the VEG1 and VEG2 simulations for corresponding climate scenarios were used to estimate the effects of climate-induced LCC on ET.

### 2.5. Statistical analysis

Root mean square error (RMSE), Nash–Sutcliffe model efficiency coefficient (NS) and mean percentage error (MPE) were used to evaluate the accuracy of ET estimates. The smaller values of RMSE and MPE, and NS close to 1 (range from −∞ to 1) indicate more accurate model estimates. The non-parametric Mann–Kendall test for trends was applied to determine significant time-series trends (Hamed and Rao, 1998).

## 3. Results and discussion

### 3.1. Evaluation of site-level ET estimates

Comparisons of site-level AL1-ET and AL2-ET estimates with measured ET at the two EC sites (Table 2, Fig. 3) indicate that the AL2 greatly outperforms AL1. The MPE of 5.94% and 6.42% for annual AL2-ET, at the SKT and KBU sites, respectively, suggests that the AL2-ET generally agrees well with measured ET at the site level. The seasonal changes of AL2-ET, GLEAM and MODIS-ET match well with the measured ET at both sites, except from November to March (Fig. 3). During the winter months, the AL2-ET and GLEAM estimates are very close to the measured ET whereas MODIS-ET estimates are much higher. The overestimation of ET by MODIS-ET during the winter is probably due to the increased uncertainties of driving data, e.g., land cover, albedo, LAI and reanalysis climate data (Strahler et al., 2002; Jin et al., 2002, 2003b; Wang et al., 2004, 2005; Gao et al., 2005; Heinsch et al., 2006; Zhao et al., 2006; Sprintsin et al., 2009; Decker et al., 2011). In contrast, AL1-ET tends to overestimate ET during the summer, which is likely due to the overestimation of PET in the summer by the AL1 (Feddes and Lenselink, 1994) and the bias is passed on to the AL1-ET.

### 3.2. Evaluation of regional ET estimates

Regional AL2-ET (regional ET was determined by summing area-weighted ET estimates across all grid cells within the study region) matches well with regional MODIS-ET and GLEAM during the growing season, and performs better than regional AL1-ET (Fig. 4). The regional AL1-ET is much higher during the growing season, especially in July (18.6–41.5% higher), which is probably due to the overestimation of ET by AL1-ET in the summer as shown in the site-level analyses (Section 3.1). In contrast, GLEAM during the growing season is similar to AL2-ET and MODIS-ET. The regional AL2-ET is lower than the regional MODIS-ET in the non-growing season (Fig. 4), which is likely due to the overestimation of MODIS-ET during this time as indicated in the site-level analyses. Overall, GLEAM reports an average annual ET of 210.07 mm $yr^{-1}$ in the region during 2000–2008, which compares well to the 223.6 mm $yr^{-1}$ by AL2-ET. Estimates by MODIS-ET (282.86 mm $yr^{-1}$) and AL1-ET (305.56 mm $yr^{-1}$) are much higher, which are likely due to their overestimation of ET in the winter and summer, respectively.

Across the plateau, the average annual AL1-ET and AL2-ET estimates over the 2000–2008 time period, show an increasing gradient from southwest to northeast that compares well with patterns observed by GLEAM and MODIS-ET (Fig. 5). At the same time, the AL1-ET of the eastern and northern parts of the plateau is obviously higher than that of MODIS-ET and GLEAM, likely because the AL1-ET is overestimated during the summer (Feddes and Lenselink, 1994) and the errors are unevenly distributed. The overall magnitude of MODIS-ET, however, is higher than that of AL1-ET and AL2-ET and the gradient of MODIS-ET across the plateau is not as strong as in the AL1-ET and AL2-ET estimates. This might be partially caused by the higher ET estimates during the winter when the monthly MODIS-ET estimates are 8–20 mm higher than those of AL1-ET and AL2-ET, and the differences are not evenly

**Table 2**
Comparison of accuracies among AL1-ET, AL2-ET, MODIS-ET and GLEAM estimates at the EC sites of SKT and KBU, a and b under each ET estimate category stand for whole measurement period and growing seasons, respectively. Low values of RMSE and higher values of NS indicate better accuracy.

| | SKT | | | | | | | | KBU | | | | | | | |
|---|---|---|---|---|---|---|---|---|---|---|---|---|---|---|---|---|
| | AL1-ET | | AL2-ET | | MODIS-ET | | GLEAM | | AL1-ET | | AL2-ET | | MODIS-ET | | GLEAM | |
| | a | b | a | b | a | b | a | b | a | b | a | b | a | b | a | b |
| RMSE (mm $mon^{-1}$) | 10.99 | 14.05 | 6.30 | 7.67 | 10.65 | 8.16 | 9.27 | 10.93 | 11.86 | 15.56 | 6.70 | 7.58 | 9.04 | 7.84 | 7.14 | 9.17 |
| NS | 0.71 | 0.51 | 0.91 | 0.89 | 0.73 | 0.82 | 0.76 | 0.62 | 0.42 | 0.13 | 0.82 | 0.76 | 0.62 | 0.73 | 0.78 | 0.68 |

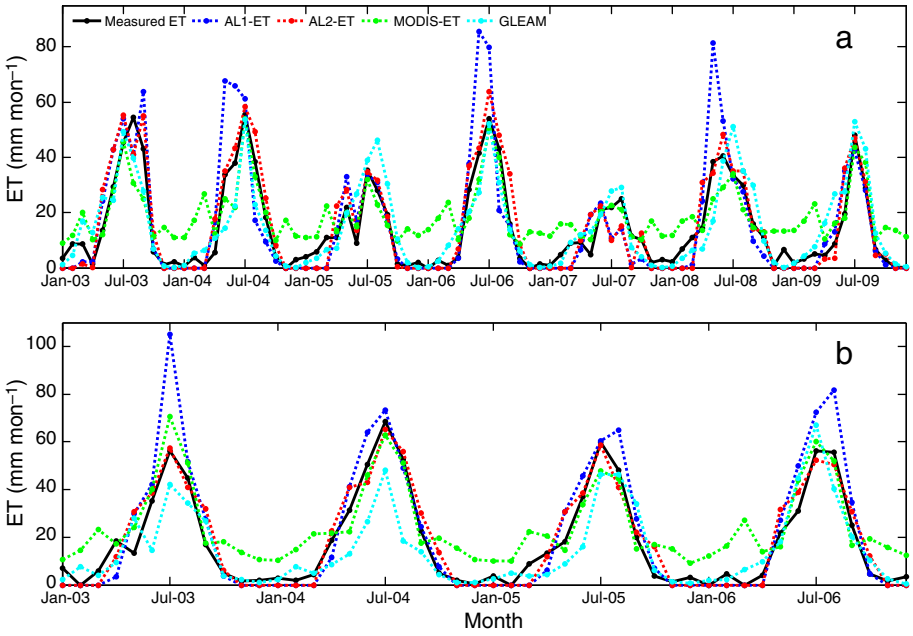


**Fig. 3.** Comparison between measured ET, AL1-ET, AL2-ET, MODIS-ET and GLEAM at: (a) KBU site, and (b) SKT site.

distributed across the plateau. Spatially, there are small differences between whole-year ET and growing season ET for AL1-ET and AL2-ET because their ET amounts in the winter are very small. However, there are notable differences when it comes to MODIS-ET because MODIS-ET in winter tends to be higher, accounting for 24.6% of the average annual ET over 2000–2008. In contrast, the PM-Mu ET estimates of Vinukollu et al. (2011) are much lower than the other ET estimates (Fig. 5), which is similar with the evaluation in the Vinukollu et al. (2011) that PM-Mu ET estimates have sizeable negative bias ($-132$ mm yr$^{-1}$ over 26 basins across continents), large discrepancy with observed data, and large RMSE. Although PM-Mu ET estimates by Vinukollu et al. (2011) and MODIS-ET are both based on PM framework, the parameterization and forcing data are different (Mu et al., 2007; Vinukollu et al., 2011). In addition, the former was based on the methods in Mu et al. (2007), whereas the latter was based on the methods in Mu et al. (2011) which further improved those of 2007. Moreover, the aerodynamic resistance in PM-Mu is calculated from Surface Energy Balance System (SEBS) model instead using the methods described in Mu et al. (2007) (Vinukollu et al., 2011). These differences may explain why PM-Mu ET estimates of Vinukollu et al. (2011) are much lower than MODIS-ET.

Due to the significant improvements demonstrated by the AL2 algorithms over the AL1 algorithms at both the site and regional levels, the AL2 algorithms were used in the TEM simulations to examine how climate change and LCC might influence ET in the future.

### 3.3. Climate change effects on ET

ET ranges from 188 mm yr$^{-1}$ to 286 mm yr$^{-1}$ across all scenarios using the VEG1 land cover during the 21st century, but increases in ET differ in magnitude among the six climate scenarios (Fig. 6, Table 3). The largest ET increases (0.55 mm yr$^{-2}$) occurred in the X903H scenario and the smallest ET increases (0.11 mm yr$^{-2}$) occurred in the X905L scenario. Larger increases in ET occurred in the scenarios based on the BAU emission policy (X903H, X901M, X902L) than in the emission stabilization policy (X906H, X904M, X905L). Within an

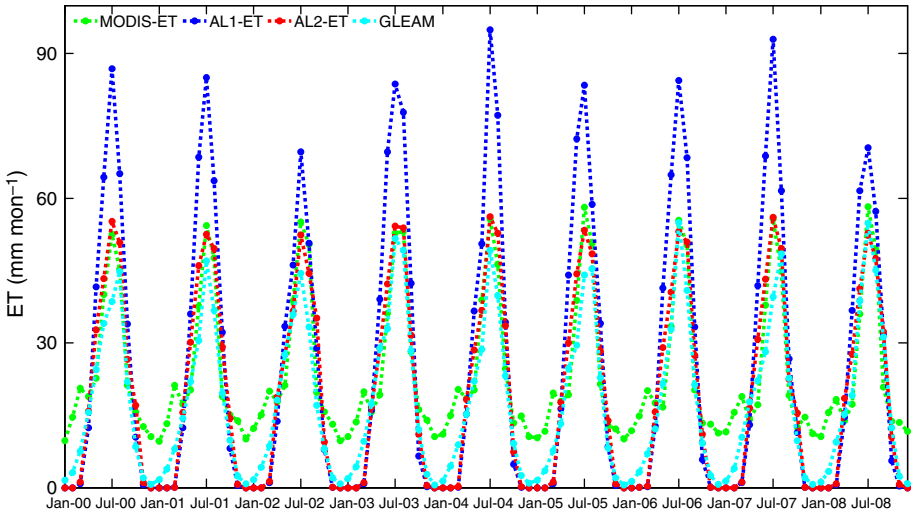


**Fig. 4.** Comparison among regional MODIS-ET, AL1-ET, AL2-ET and GLEAM during 2000–2008.

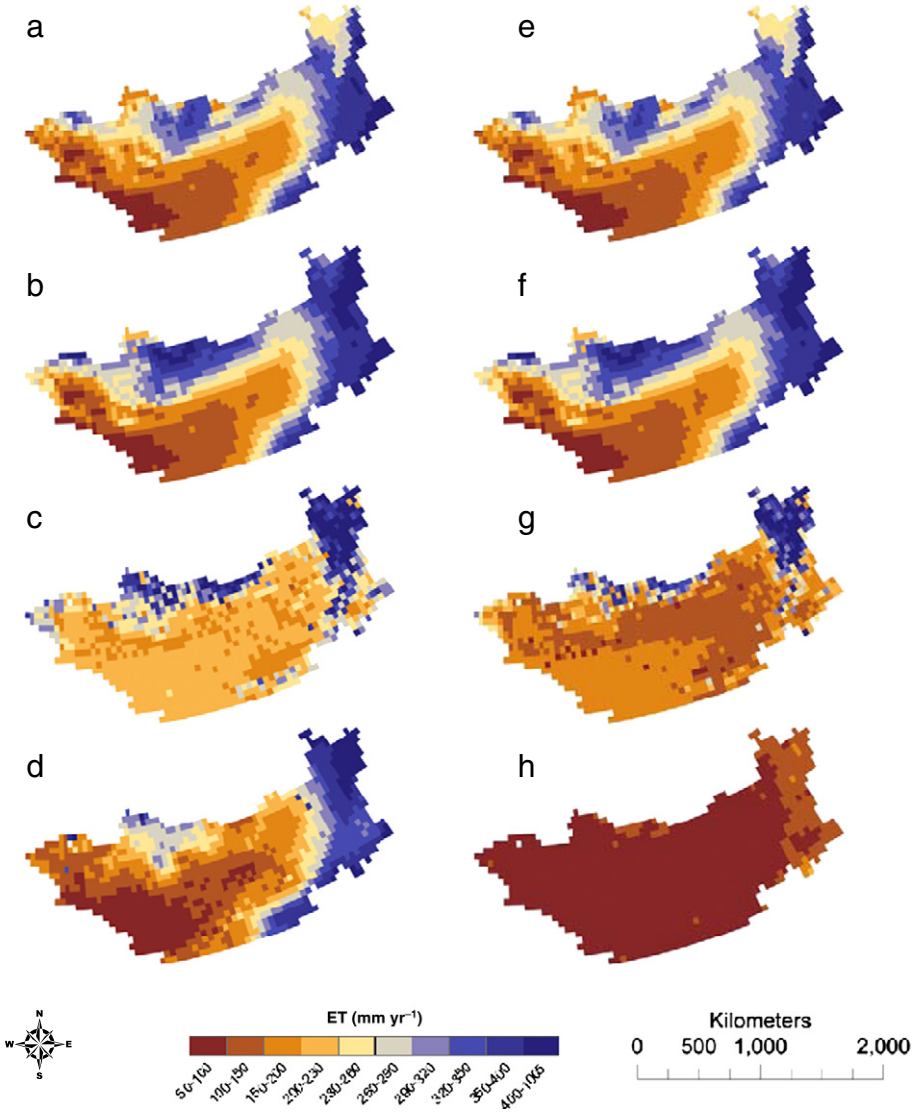


**Fig. 5.** Spatial pattern of average annual ET over 2000–2008 derived from (a) AL2, (b) AL1, (c)MODIS, and (d) GLEAM, and average growing season ET over 2000–2008 derived from (e) AL2, (f) AL1, (g) MODIS, and (h) average annual PM-Mu ET over 2000–2007 in Vinukollu et al. (2011).

emission policy, higher ET and larger increases in ET occurred in the climate scenarios that had a higher climate response than a lower climate response (X903H > X901M > X902L > X906H > X904M > X905L). Moreover, the order of ET estimates among the climate scenarios is also consistent with the projected increases in air temperature and precipitation among the climate scenarios (Table 3, Fig. 1). Higher precipitation would increase the supply of water for ET whereas higher air temperatures would increase atmospheric demand for water vapor by increasing the vapor pressure deficit (Anderson, 1936). Thus, our results indicate that the water cycling on the plateau will intensify in the future, but the level of this intensification will depend on the climate policy being implemented and the response of climate to greenhouse gas forcings.

The southwest to northeast gradient in ET is projected to continue to exist in the future in all six scenarios following a similar gradient in precipitation (Fig. 7). However, the spatial patterns of changes in AL2-ET vary among the climate scenarios. In the BAU emission scenarios, AL2-ET increases almost over the entire region (Fig. 8). In contrast, AL2-ET decreases in some regions of the plateau and increases in other regions in the level-one stabilization emission scenarios. Furthermore, the southwestern region, where the land cover is predominantly semi-desert/desert (Fig. 2), has the smallest increases in AL2-ET from the 1990s to 2090s in all scenarios.

Land cover influences both the rate of ET and the relative importance of ET to water cycle, which may be represented as a ratio of ET to precipitation (ET/P). Grasslands, boreal forests and semi-desert/deserts account for 90% of the vegetated area in the region. For all scenarios, the regional grassland ET ranges from 242 to 374 mm $yr^{-1}$ (Table 4 and Fig. 9), with an average ET/P of 90%, which coincides with that at the KBU grassland site. Regional boreal forest ET ranges from 213 to 278 mm $yr^{-1}$, with an average ET/P of 72%, which falls in the range of ratio at the boreal forest site SKT (70%–89%). The semi-desert/desert ET varies from 100 to 199 mm $yr^{-1}$ and accounts for 95–100% of the precipitation, which is consistent with previous studies in arid areas (Kurc and Small, 2004; Sun et al., 2011a; Katul et al., 2012; Wang and Dickinson, 2012), and the average regional semidesert/desert ET ~145 mm $yr^{-1}$ during 21st century for all scenarios is comparable to the current average estimates for these ecosystems (Jiménez et al., 2011; Miralles et al., 2011a). The simulated ET differences for various land cover types are mainly due to the climate variations across different land covers, e.g., the precipitation and air temperature in the grassland being higher than those of the boreal

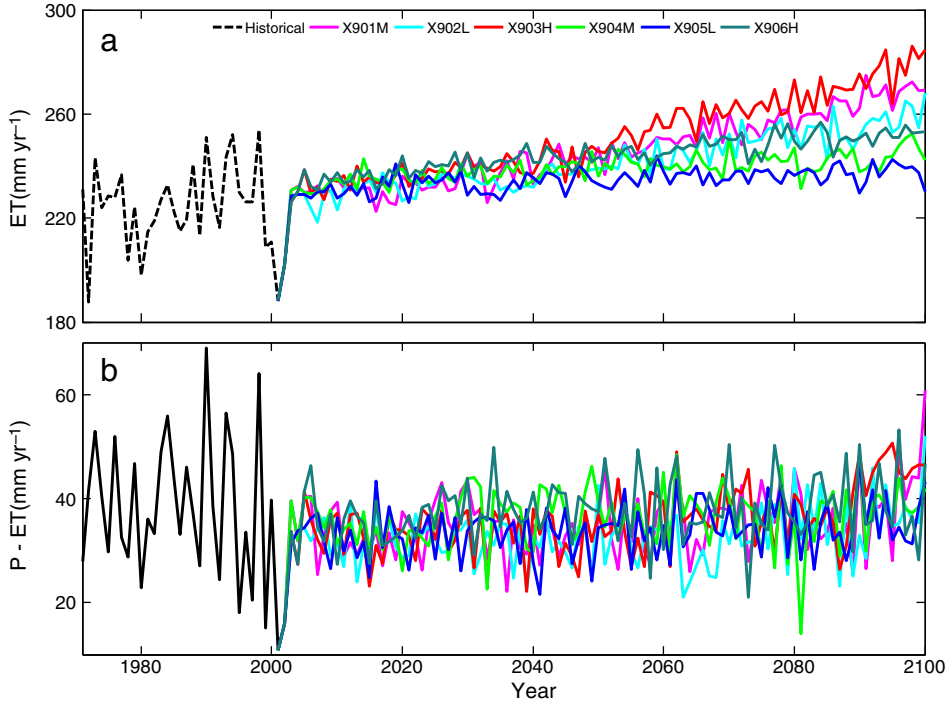


**Fig. 6.** ET and P-ET variations over 1971–2100 under VEG1 in X901M, X902L, X903H, X904M, X905L, and X906H: (a) annual regional AL2-ET, and (b) annual regional P-ET.

forest, or precipitation in the semidesert/desert being lower than that of the grassland or boreal forest. In particular, in the X903H scenario, precipitation during the growing season in grasslands is 23 mm higher than that of the boreal forest, 190 mm higher than that of the semidesert/desert, and the mean air temperature during the growing season in grasslands is 5.34 °C higher than that of the boreal forest.

### 3.4. Land cover effects on ET

The regional AL2-ET estimates using the VEG2 land cover were slightly higher than the estimates using the VEG1 land cover in all six scenarios (Fig. 10). The differences in ET between the two land cover scenarios are more apparent in the BAU emission scenarios than in the level-one stabilization emission scenarios, but these differences are <5% of the AL2-ET estimates using the VEG1 land cover. Likewise, LCC appeared to have subtle effects on the spatial distribution of AL2-ET (Figs. 7–8). Thus, the direct effects of climate change on ET appeared to be more important than the indirect effects of climate-induced LCC on ET.

There are two possible reasons for the inconspicuous effects of LCC on ET. First, the positive response of ET to LCC in some areas is offset by the negative response in other areas and, as a result, the change of aggregated ET over the whole plateau is small. The positive effect includes the change from forest to grassland, and the negative effect is due to the change from forest and grassland to semidesert/desert and from grassland to forest. For example, in the X903H scenario with the largest LCC among the six scenarios, the boreal forests and temperate forests will largely become grasslands and the semidesert/desert coverage will expand from 34.5% to 50% of the plateau by the end of the 21st century, specifically, 20.1% of the vegetated area will change from forests to grassland and 14.5% will change from grassland to semidesert/desert. Furthermore, the change area in all scenarios accounts for only 9–36% of the total area (Fig. 2). These relatively small changes in land cover appeared to have subtle effects on the spatial distribution of ET and regional ET estimates.

**Table 3**
Range (mm $yr^{-1}$) and increasing trends (mm $yr^{-2}$) of regional annual AL2-ET, AL1-ET, and precipitation of Mongolia in the 21st century in X901M, X902L, X903H, X904M, X905L, and X906H under VEG1.

| | AL2-ET | | Precipitation | |
|---|---|---|---|---|
| | Range | Trend | Range | Trend |
| X901M | 188–275 | 0.47 | 199–330 | 0.38 |
| X902L | 188–268 | 0.38 | 199–320 | 0.28 |
| X903H | 188–286 | 0.55 | 199–334 | 0.48 |
| X904M | 188–252 | 0.17 | 199–292 | 0.18 |
| X905L | 188–244 | 0.11 | 199–284 | 0.12 |
| X906H | 188–257 | 0.25 | 199–306 | 0.28 |

Note: for all the trend analyses, $P < 0.001$.

### 3.5. Implications of projected ET trends on the water availability

It is becoming recognized that water availability is a crucial limiting natural resource for human development, especially in arid and semiarid areas (Vorosmarty et al., 2000; Fekete et al., 2004). Our simulation results indicate that annual mean volumetric soil moisture varies very slightly from year to year, with trends ranging from $-0.0069\%$ to $-0.021\%$ $yr^{-1}$ in all scenarios. Because the variation of soil moisture is negligible over the long run, net precipitation, the difference between precipitation and ET (hereafter P-ET), can approximately represent water availability, in other words, how much water may be available for human use.

Regional P-ET fluctuates without a significant trend in all the scenarios using the VEG1 land cover during the 21st century (Fig. 6). In addition, changes in P-ET from the 1990s to 2090s ($\Delta$(P-ET)) are insignificant ($\pm 20$ mm) across most of the plateau (Fig. 8). These results imply that without considering further anthropogenic impacts, projected climate change itself will not significantly increase threats to the water availability as increasing ET rates are being compensated by increasing precipitation rates. However, the threats to the water availability differ from scenario to scenario due to inconsistent trends between ET and precipitation. With the VEG1 land cover, P-ET will increase from the 1990s to 2090s across a large portion of the plateau (Fig. 8) with larger changes in the BAU scenarios (X901M: 10.4 mm

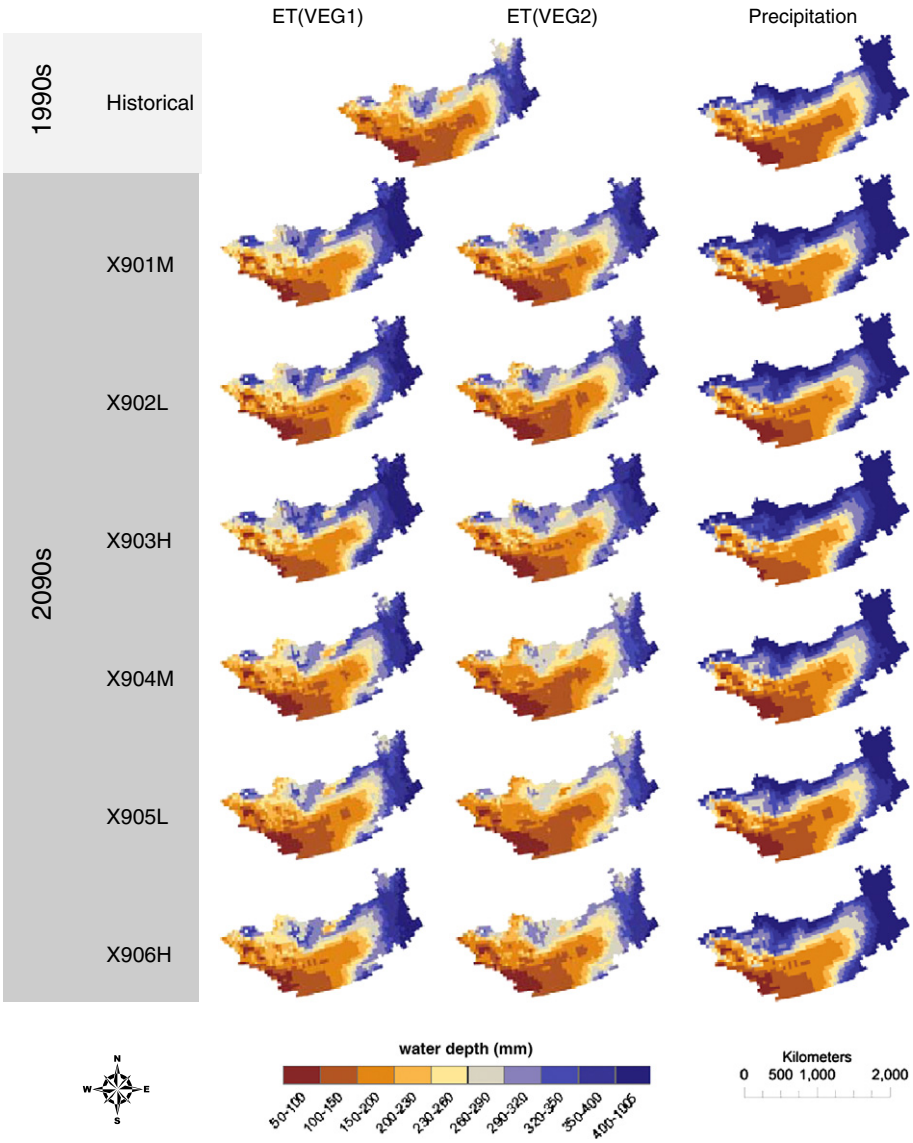


**Fig. 7.** Spatial patterns of average annual AL2-ET (under VEG1 and VEG2) and precipitation over the 1990s and the 2090s in X901M, X902L, X903H, X904M, X905L, and X906H.

or +58.3%; X902L: 2.4 mm or +52.8%; X903H: 5.4 mm or +56.9%) than the stabilized emission scenarios (X904M: 2.5 mm or +49.6%; X905L: 0.4 mm or +48.9%; X906H: 2.8 mm or +51.5%). These results suggest that, as a whole, the BAU emission scenarios tend to have slightly more available water for human use and less area will be threatened by water shortage relative to the level one stabilization emission scenarios.

With climate-induced LCC, fewer areas are likely to suffer from water shortage, although the increase in average P-ET from the 1990s to the 2090s using the VEG2 is slightly less than that using the VEG1 (Fig. 8). This discrepancy is likely due to the uneven effects of LCC across the plateau. At the same time, one common feature across all the scenarios is that future water supplies tend to be threatened in the northeastern part of the plateau where boreal forests are currently located.

### 3.6. Model limitations and simulation uncertainties

ET estimation is challenging because it involves a large number of biophysical factors such as landscape heterogeneity, plant biophysics for specific species, leaf angle, canopy structure, soil properties, soil moisture, and microclimate (ASCE, American Society of Civil Engineers, 1996; Wang et al., 2010; Mu et al., 2011). The algorithms used in this study do not account for biodiversity effects, as different species within a single plant functional type can have different ET rates that also vary with stand age. Uncertainties also exist in a number of the biophysical parameters in the AL2 algorithms, and all parameters are assumed to have the same value for a given biome type across the entire plateau. Moreover, the algorithms for soil evaporation are based on an assumption that SM has a strong link with the adjacent atmospheric moisture during an entire month, whereas the strongest link occurs at midday during convective conditions (Fisher et al., 2008). The application of the model at a monthly step might then contribute to ET errors. Another limitation of the algorithms is that the effect of high-$CO_2$-induced partial stomatal closure on stomatal resistance (Jarvis, 1976; Gedney et al., 2006; Lammertsma et al., 2011; Miglietta et al., 2011) has not been taken into account. Although the influence of available water on stomatal closure has been considered in the simulation of atmospheric $CO_2$ fertilization effects on gross primary production (Raich et al., 1991; McGuire et al., 1997; Zhuang et al., 2003), the corresponding influence of $CO_2$ on partial stomatal closure has not been considered in simulating ET and needs to be examined in future work.

ET is very sensitive to short-term weather conditions (ASCE, American Society of Civil Engineers, 1996 Allen et al., 1998) so the input of relatively coarse monthly meteorological data into TEM may

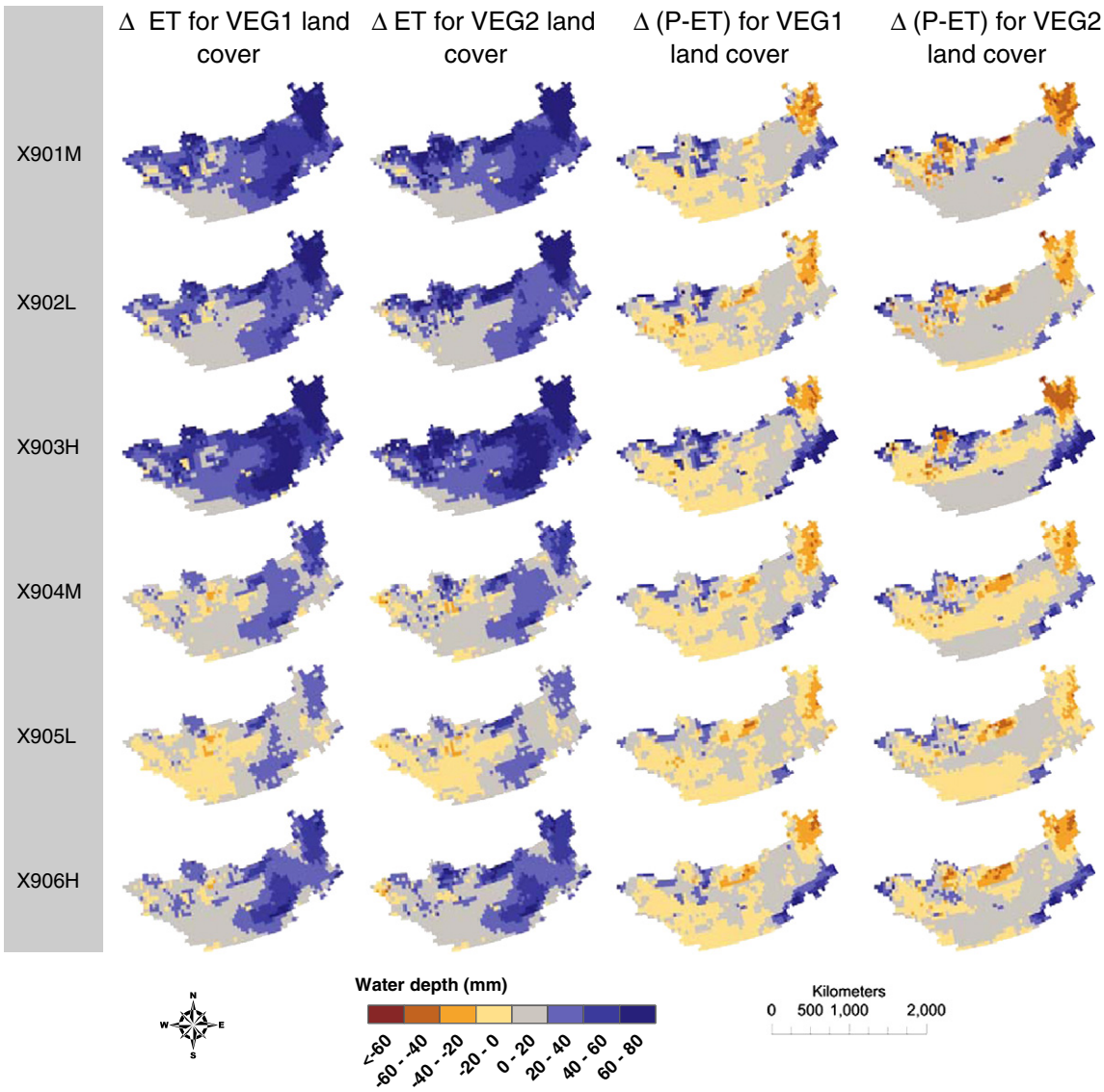


**Fig. 8.** Spatial patterns of changes in average annual AL2-ET and net precipitation from the 1990s to the 2090s, using VEG1 and VEG2 land covers and X901M, X902L, X903H, X904M, X905L, and X906H climate scenarios.

bias ET estimates. In addition, the omission of some processes such as snow sublimation, evaporation from wet canopy surface, and wet soil surface will also lead to underestimation of total ET. In the case of forested regions, the omission of wet canopy evaporation may lead to an underestimation of ET, as the rates of interception loss may overcome several times those of transpiration (Gash and Shuttleworth, 2007; Miralles et al., 2010). The AL2-ET during the non-growing season is underestimated (Fig. 3), because the LAI is estimated to be zero by TEM in most cases during this period, which results in transpiration being zero. Low vapor pressure leads to low RH during this period, which also results in low soil evaporation (see Eqs. (2c, 2d and 2e)). Then, a daily version of the TEM that has incorporated with the aforementioned processes and improvements on LAI and soil evaporation may produce better ET estimates.

**Table 4**
Range (mm $yr^{-1}$) and increasing trends (mm $yr^{-1}$) of annual grassland ET, boreal forest ET, and semidesert/desert ET of Mongolia in the 21st century in X901M, X902L, X903H, X904M, X905L, and X906H.

| | Grass | | Boreal forest | | Semidesert/desert | |
|---|---|---|---|---|---|---|
| | Range | Trend | Range | Trend | Range | Trend |
| X901M | 242–355 | 0.60 | 218–270 | 0.26 | 100–179 | 0.34 |
| X902L | 242–350 | 0.48 | 217–264 | 0.20 | 100–172 | 0.28 |
| X903H | 242–374 | 0.67 | 213–278 | 0.29 | 100–199 | 0.38 |
| X904M | 242–332 | 0.20 | 215–246 | 0.10 | 100–170 | 0.15 |
| X905L | 242–322 | 0.17 | 213–242 | 0.06 | 100–158 | 0.10 |
| X906H | 242–335 | 0.32 | 213–251 | 0.13 | 100–175 | 0.19 |

Note: for all the trend analyses, $P < 0.001$.

All input driving data for the TEM have inherent uncertainties (Zobler, 1986; Webster et al., 2002; Mitchell and Jones, 2005; Sokolov et al., 2005; Farr, 2007). Spatially-interpolated CRU climate data are based on sparse and irregular meteorological stations in this region (New et al., 1999; New et al., 2000; Mitchell and Jones, 2005;), whereas climate and terrain conditions vary in this region, the CRU data therefore have inherent uncertainties. The reanalysis ECMWF data and IGSM scenario climate data were simulated by models (Sokolov et al., 2005; Dee et al., 2011) so that the innate uncertainties in the model outputs will be inherited into the TEM ET estimation. Further, the VEG2 data are not continuously changing over time, our assumption that land cover remains the same over a period of 25 years may result in further errors. A data set with more continuous changes in land cover over

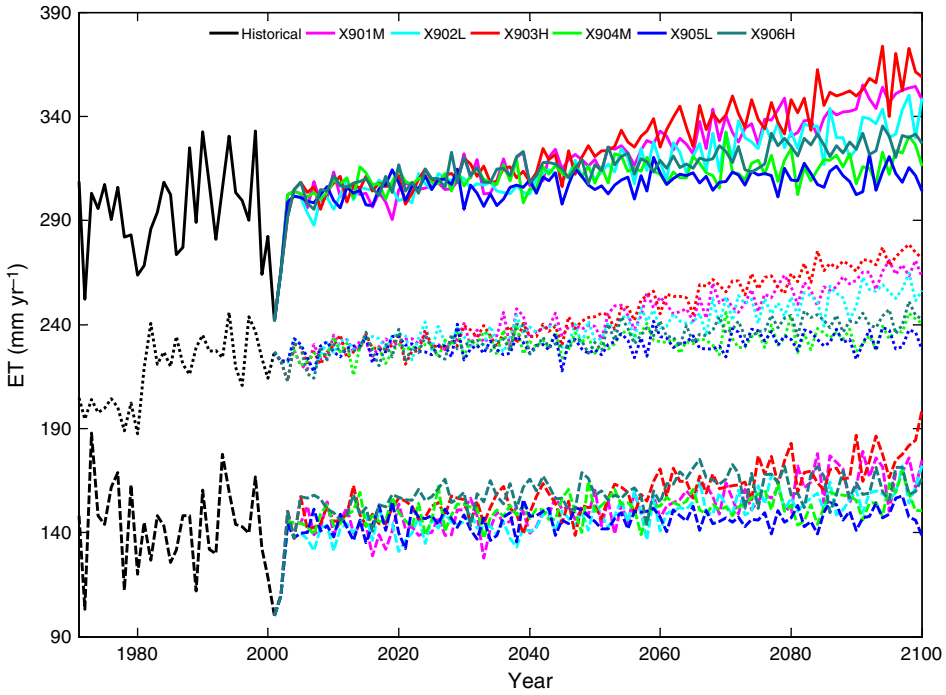


**Fig. 9.** Annual regional grassland ET, boreal forest ET, and semidesert/desert ET variation over the period of 1971–2100 in X901M, X902L, X903H, X904M, X905L, and X906H under VEG1 (grassland ET — solid line; boreal forest ET — dotted line; semidesert/desert ET — dashed line).

the 21st century would improve the prediction of ET for future scenarios.

EC tower measurements used for validation also have different sources of uncertainty. Flux measurements are often affected by systematic errors such as energy balance disclosure and incomplete measurement of nocturnal flux exchange (Aubinet et al., 1999; Hollinger and Richardson, 2005). Energy closure imbalance is common in eddy covariance studies and varies from a small percentage to 30–40% as a result of limitations in instrumentation, spatial heterogeneity of EC footprints, and the partial shortage of measured turbulent and advective fluxes (Anthoni et al., 1999; Wilson et al., 2002; Tchebakova et al., 2002). Further, there is likely a spatial-scale mismatch between the source area of the available energy (i.e. $R_n$ − G) and the turbulent flux source areas (Schmid, 1994, 1997; Schmid and Lloyd, 1999; Scott, 2010). For example, the source area of the available energy derived from ridge-top locations may be mismatched with

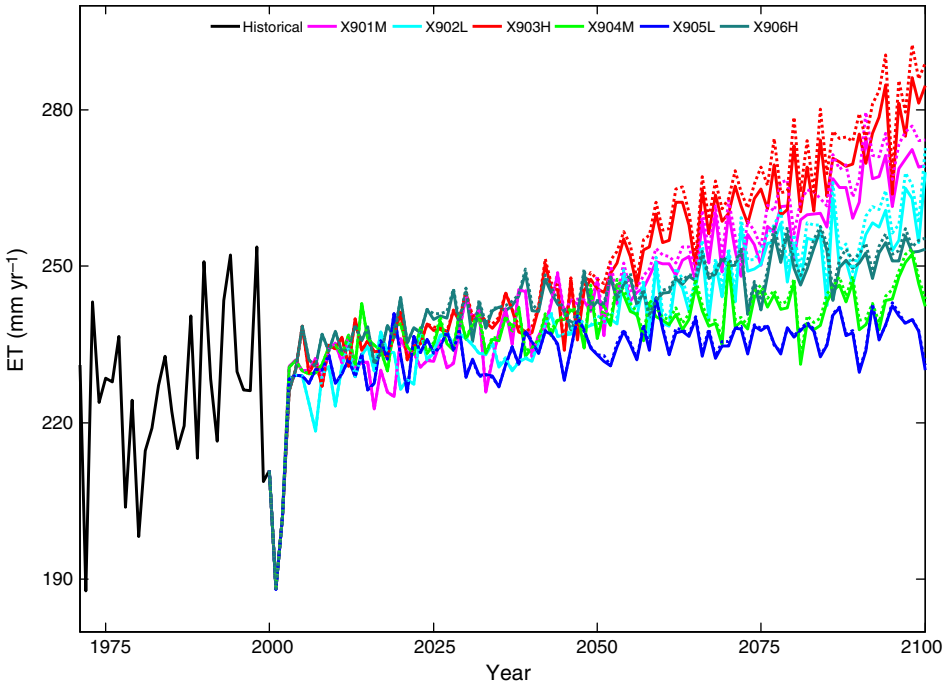


**Fig. 10.** Annual regional ET variations over the period 1971–2100 under VEG1 and VEG2 (VEG1 — solid line; VEG2 — dotted line) in X901M, X902L, X903H, X904M, X905L, and X906H.

the fluctuating turbulent flux source areas, which are often located on sloped surfaces with varied aspects (Schmid, 1994; Scott, 2010). Moreover, all EC systems attenuate the true turbulent signals at sufficiently high and low frequencies, especially at night (Moore, 1986; Massmana and Lee, 2002). As a result, ET estimates from the EC towers have uncertainties ranging 10–30% (Glenn et al., 2008).

Finally the satellite-based ET estimates used here for comparison (e.g. MODIS-ET, GLEAM and the PM-Mu ET by Vinukollu et al, 2011) have uncertainties that are either cascaded from the inputs used to drive the methods or inherent to the algorithms themselves. This study has revealed potential uncertainties of MODIS ET during the winter on the plateau. The input climate data of the Global Modeling and Assimilation Office (GMAO) re-analyses used to drive MODIS-ET tends to have high uncertainties in winter (Zhao et al., 2006; Decker et al., 2011). Other possible error sources lie in the input MODIS land cover data, where the accuracies are in the range of 70–80% (Strahler et al., 2002), and the inherited uncertainties from the MODIS albedo (MOD43C1). The uncertainties of albedo in the winter are especially distinct on the plateau since it is dominated by grassland (Fig. 2) and its albedo is most sensitive to snow cover when compared with other land cover (Jin et al., 2002, 2003b; Gao et al., 2005). An additional potential source of error is the input MODIS LAI, which tends to overestimate (Wang et al., 2004; Heinsch et al., 2006). The uncertainties in the MODIS land cover and albedo will propagate to the MODIS LAI in addition to their direct impacts on MODIS ET (Yang et al., 2006; Sprintsin et al., 2009). Some studies show that MODIS LAI has more apparent uncertainties in winter relative to summer (Wang et al., 2005; Sprintsin et al., 2009).

## 4. Conclusions

Despite the deficiencies and uncertainties of our model simulations described above, our analyses indicates that the modified TEM captures current spatial and temporal variations in ET as well as, or better than other approaches, and provides helpful insights about how ET and water availability on the Mongolian Plateau may change in the future in response to climate change and climate-induced LCC.

For the three dominant land cover types on the plateau, ET is all projected to increase. Grasslands have the highest regional annual ET, followed by the boreal forest and semi-desert/desert, whereas the increasing trends of ET are highest at grassland and lowest in boreal forest. The spatial gradients of annual ET across the plateau are expected to remain throughout the 21st century, increasing from the southwestern region to the northeastern region.

The magnitude and spatial pattern of changes in ET will depend on the climate policy being implemented and the sensitivity of climate to the energy forcing from greenhouse gas emissions. Larger changes in ET are expected from a BAU policy than a policy that attempts to stabilize greenhouse gas emissions as a result of larger changes in precipitation and air temperatures under the BAU policy. Furthermore, ET is expected to increase across most of the Mongolian Plateau under the BAU policy whereas ET will increase in some regions but decrease in other regions under a level-one stabilization emission policy. Under both policies, a larger climate response to greenhouse gas forcing is expected to result in larger increases in ET. The enhanced ET is not expected to threaten water availability across most of the Mongolian Plateau because of concurrent increases in projected precipitation. An exception, however, may be the north-central and northeastern parts of the plateau where large decreases in net precipitation are projected to occur in some climate scenarios.

Climate-induced changes in land cover are expected to have only minor effects on future regional ET with most of the regional ET changes (>95%) resulting directly from climate changes. Nevertheless, climate-induced LCC will induce visible changes in spatial distribution of net precipitation across the plateau during the 21st century, suggesting that future ET and water availability studies over time period of decades may need to consider the effects of LCC on ET.

## Acknowledgment

This research is supported by the NASA Land Use and Land Cover Change program (NASA-NNX09AI26G, NN-H-04-Z-YS-005-N, and NNX09AM55G), the Department of Energy (DE-FG02-08ER64599), the National Science Foundation (NSF-1028291 and NSF-0919331), and the NSF Carbon and Water in the Earth Program (NSF-0630319). The computing is supported by the Rosen Center of High Performance Computing at Purdue University. Special acknowledgment is made here to Prof. Eric Wood of Princeton University for his generous provision of ET dataset in the Vinukollu et al. (2011). Diego Miralles acknowledges the support by the European Space Agency WACMOS-ET project (contract no. 4000106711/12/I-NB).

## References

Allen, R.G., Pereira, L.S., Raes, D., Smith, M., 1998. Crop Evapotranspiration—Guidelines for Computing Crop Water Requirements—FAO Irrigation and Drainage Paper 56. FAO, Rome (328 pp.).
Anderson, D.B., 1936. Relative humidity or vapor pressure deficit. Ecology 17 (2), 277–282.
Anthoni, P.M., Law, B.E., Unsworth, M.H., 1999. Carbon and water vapor exchange of an open-canopied ponderosa pine ecosystem. Agricultural and Forest Meteorology 95 (3), 151–168.
ASCE (American Society of Civil Engineers), 1996. Hydrology Handbook. ASCE Manuals and Reports on Engineering Practice, 28. ASCE, New York.
Aubinet, M., Grelle, A., Ibrom, A., Rannik, Ü., Moncrieff, J., Foken, T., Kowalski, A.S., Martin, P.H., Berbigier, P., Bernhofer, C., 1999. Estimates of the annual net carbon and water exchange of forests: the EUROFLUX methodology. Advances in Ecological Research 30, 113–175.
Ball, J.T., 1987. A model predicting stomatal conductance and its contribution to the control of photosynthesis under different environmental conditions. Prog. Photosynthesis Res. Proc. Int. Congress 7th, Providence. 10–15 Aug 1986, Vol. 4. Kluwer, Boston, pp. 221–224.
Barnett, T.P., Adam, J.C., Lettenmaier, D.P., 2005. Potential impacts of a warming climate on water availability in snow-dominated regions. Nature 438 (7066), 303–309.
Bates, B., Kundzewicz, Z.W., Wu, S., Palutikof, J., 2008. Climate change and water. Intergovernmental Panel on Climate Change (IPCC).
Betts, A.K., Ball, J.H., Beljaars, A.M., Miller, M.J., Viterbo, P.A., 1996. The land surface-atmosphere interaction: a review based on observational and global modeling perspectives. Journal of Geophysical Research 101 (D3), 7209.
Bonan, G., 2008. Ecological Climatology, Concepts and Applications. Cambridge University Press, New York 690.
Bouchet, R.J., 1963. Evapotranspiration réelle et potentielle, signification climatique. IAHS Publ. 62, 134–142.
Chen, B., Ge, Q., Fu, D., Liu, G., Yu, G., Sun, X., Wang, S., Wang, H., 2009. Upscaling of gross ecosystem production to the landscape scale using multi-temporal Landsat images, eddy covariance measurements and a footprint model. Biogeosciences Discussions 6, 11317–11345.
Chen, Z., Zhang, X., Cui, M., He, X., Ding, W., Peng, J., 2012. Tree-ring based precipitation reconstruction for the forest–steppe ecotone in northern Inner Mongolia, China and its linkages to the Pacific Ocean variability. Global and Planetary Change 86, 45–56.
Cleugh, H.A., Leuning, R., Mu, Q., Running, S.W., 2007. Regional evaporation estimates from flux tower and MODIS satellite data. Remote Sensing of Environment 106 (3), 285–304.
Decker, M., Brunke, M.A., Wang, Z., Sakaguchi, K., Zeng, X., Bosilovich, M.G., 2011. Evaluation of the reanalysis products from GSFC, NCEP, and ECMWF using flux tower observations. Journal of Climate 25, 1916–1944.
Dee, D.P., et al., 2011. The ERA-Interim reanalysis: configuration and performance of the data assimilation system. Quarterly Journal of the Royal Meteorological Society 137 (656), 553–597.
Dickinson, R.E., Shaikh, M., Bryant, R., Graumlich, L., 1998. Interactive canopies for a climate model. Journal of Climate 11 (11), 2823–2836.
Dolman, A.J., De Jeu, R., 2010. Evaporation in focus. Nature Geoscience 3 (5), 296.
Dolman, A.J., Gash, J.H., Roberts, J., Shuttleworth, W.J., 1991. Stomatal and surface conductance of tropical rainforest. Agricultural and Forest Meteorology 54 (2), 303–318.
Dulamsuren, C., Hauck, M., Mühlenberg, M., 2009. Ground vegetation in the Mongolian taiga forest-steppe ecotone does not offer evidence for the human origin of grasslands. Applied Vegetation Science 8 (2), 149–154.
FAO (Food and Agriculture Organization of the United Nations), 1971. Soil map of the world. UNESCO, Paris.
Farr, T.G., 2007. The shuttle radar topography mission. Reviews of Geophysics and Space Physics 45, RG2004.
Feddes, R.A., Lenselink, K.J., 1994. Evapotranspiration. In: Ritzema, H.P. (Ed.), Drainage Principles and Applications. Water Resources Pubns, Wageningen, The Netherlands, p. 1125.

Fekete, B.M., Vörösmarty, C.J., Roads, J.O., Willmott, C.J., 2004. Uncertainties in precipitation and their impacts on runoff estimates. Journal of Climate 17 (2), 294–304.
Fisher, J.B., Tu, K.P., Baldocchi, D.D., 2008. Global estimates of the land–atmosphere water flux based on monthly AVHRR and ISLSCP-II data, validated at 16 FLUXNET sites. Remote Sensing of Environment 112 (3), 901–919.
Galloway, J., Melillo, J., 1998. Asian Change in the Context of Global Climate Change: Impact of Natural and Anthropogenic Changes in Asia on Global Biogeochemical Cycles, 3. Cambridge University Press.
Gao, F., Schaaf, C.B., Strahler, A.H., Roesch, A., Lucht, W., Dickinson, R., 2005. MODIS bidirectional reflectance distribution function and albedo Climate Modeling Grid products and the variability of albedo for major global vegetation types. Journal of Geophysical Research 110 (D01104), 2005.
Garnier, E., Cordonnier, P., Guillerm, J.L., Sonié, L., 1997. Specific leaf area and leaf nitrogen concentration in annual and perennial grass species growing in Mediterranean old-fields. Oecologia 111 (4), 490–498.
Gash, J.H., Shuttleworth, W.J., 2007. Vegetation controls on evaporation — commentary. Benchmark Papers in Hydrology: Evaporation. IAHS Press, Wallingford (233-239 pp.).
Gedney, N., Cox, P.M., Betts, R.A., Boucher, O., Huntingford, C., Stott, P.A., 2006. Detection of a direct carbon dioxide effect in continental river runoff records. Nature 439 (7078), 835–838.
Glenn, E.P., Morino, K., Didan, K., Jordan, F., Carroll, C.K., Nagler, P.L., Hultine, K., Sheader, L., Waugh, J., 2008. Scaling sap flux measurements of grazed and ungrazed shrub communities with fine and coarse-resolution remote sensing. Ecohydrology 1 (4), 316–329.
Groisman, P., Gutman, G., Reissell, A., 2010. Introduction: climate and land-cover changes in the Arctic. In: Gutman, G., Reissell, A. (Eds.), Eurasian Arctic Land Cover and Land Use in a Changing Climate. Springer, New York, pp. 1–8.
Hamed, K.H., Rao, A.R., 1998. A modified Mann–Kendall trend test for autocorrelated data. Journal of Hydrology 204, 182–196.
Hansen, J., Nazarenko, L., Ruedy, R., Sato, M., Willis, J., Del Genio, A., Koch, D., Lacis, A., Lo, K., Menon, S., 2005. Earth's energy imbalance: confirmation and implications. Science 308 (5727), 1431–1435.
He, J., Kuhn, N., Zhang, X., Zhang, X., Li, H., 2009. Effects of 10 years of conservation tillage on soil properties and productivity in the farming–pastoral ecotone of Inner Mongolia, China. Soil Use and Management 25 (2), 201–209.
Heinsch, F.A., Zhao, M., Running, S.W., Kimball, J.S., Nemani, R.R., Davis, K.J., Bolstad, P.V., Cook, B.D., Desai, A.R., Ricciuto, D.M., 2006. Evaluation of remote sensing based terrestrial productivity from MODIS using regional tower eddy flux network observations. IEEE Transactions on Geoscience and Remote Sensing 44 (7), 1908–1925.
Hollinger, D.Y., Richardson, A.D., 2005. Uncertainty in eddy covariance and its application to physiological models. Tree Physiology 25, 873–885.
Hu, J., Su, Y., Tan, B., Huang, D., Yang, W., Schull, M., Bull, M.A., Martonchik, J.V., Diner, D.J., Knyazikhin, Y., Myneni, R.B., 2007. Analysis of the MISR LAI/FPAR product for spatial and temporal coverage, accuracy and consistency. Remote Sensing of Environment 107 (1–2), 334–347.
Huxman, T.E., et al., 2005. Ecohydrological implications of woody plant encroachment. Ecology 86 (2), 308–319.
IPCC (Intergovernmental Panel on Climate Change), 2007. Climate Change 2007: Synthesis Report. Cambridge Univ, Press, Cambridge.
IPCC(Intergovernmental Panel on Climate Change), 2001. Climate change 2001: the scientific basis. Contribution of Working Group I to the Third Assessment Report of the Intergovernmental Panel on Climate Change. Cambridge University Press, New York, USA, p. 881.
Jarvis, P.G., 1976. The interpretation of the variations in leaf water potential and stomatal conductance found in canopies in the field. Philosophical Transactions of the Royal Society of London. Series B, Biological Sciences 273 (927), 593–610.
Jensen, M.E., Haise, H.R., 1963. Estimating evapotranspiration from solar radiation. Proceedings of the American Society of Civil Engineers, Journal of the Irrigation and Drainage Division. 89, 15–41.
Jiang, L., Islam, S., Guo, W., Singh Jutla, A., Senarath, S.U.S., Ramsay, B.H., Eltahir, E., 2009. A satellite-based daily actual evapotranspiration estimation algorithm over South Florida. Global and Planetary Change 67 (1–2), 62–77.
Jiang, Y., Zhuang, Q., Schaphoff, S., Sitch, S., Sokolov, A., Kicklighter, D., Melillo, J., 2012. Uncertainty analysis of vegetation distribution in the northern high latitudes during the 21st century with a dynamic vegetation model. Ecology and Evolution 2 (3), 593–614.
Jiménez, C., et al., 2011. Global intercomparison of 12 land surface heat flux estimates. Journal of Geophysical Research-Atmospheres (1984–2012) 116 (D2).
Jin, Y., Schaaf, C.B., Gao, F., Li, X., Strahler, A.H., Zeng, X., Dickinson, R.E., 2002. How does snow impact the albedo of vegetated land surfaces as analyzed with MODIS data? Geophysical Research Letters 29 (10).
Jin, Y., Schaaf, C.B., Woodcock, C.E., Gao, F., Li, X., Strahler, A.H., Lucht, W., Liang, S., 2003a. Consistency of MODIS surface bidirectional reflectance distribution function and albedo retrievals: 1. Algorithm performance. Journal of Geophysical Research 108 (D5).
Jin, Y., Schaaf, C.B., Woodcock, C.E., Gao, F., Li, X., Strahler, A.H., Lucht, W., Liang, S., 2003b. Consistency of MODIS surface bidirectional reflectance distribution function and albedo retrievals: 2. Validation. Journal of Geophysical Research 108 (D5).
Jung, M., et al., 2010. Recent decline in the global land evapotranspiration trend due to limited moisture supply. Nature 467 (7318), 951–954.
Katul, G.G., Oren, R., Manzoni, S., Higgins, C., Parlange, M.B., 2012. Evapotranspiration: a process driving mass transport and energy exchange in the soil–plant–atmosphere–climate system. Reviews of Geophysics 50, RG3002.
Keeling, C.D., Whorf, T.P., 2005. Atmospheric $CO_2$ records from sites in the SIO air sampling network. Trends: A Compendium of Data on Global Change. Carbon Dioxide Information Analysis Center, Oak Ridge National Laboratory, Oak Ridge, TN, pp. 16–26.
Kurc, A.S., Small, E.E., 2004. Dynamics of evapotranspiration in semiarid grassland and shrubland ecosystems during the summer monsoon season, central New Mexico. Water Resources Research 40 (9).
Lammertsma, E.I., et al., 2011. Global $CO_2$ rise leads to reduced maximum stomatal conductance in Florida vegetation. Proceedings of the National Academy of Sciences 108 (10), 4035–4040.
Landsberg, J.J., Gower, S.T., 1996. Applications of Physiological Ecology to Forest Management. Academic Press.
Lean, J., Bunton, C.B., Nobre, C.A., Rowntree, P.R., 1995. The simulated impact of Amazonian deforestation on climate using measured ABRACOS vegetation characteristics. In Amazonian Deforestation and Climate. Wiley, Chichester, UK.
Li, S., Eugster, W., Asanuma, J., Kotani, A., Davaa, G., Oyunbaatar, D., Sugita, M., 2008. Response of gross ecosystem productivity, light use efficiency, and water use efficiency of Mongolian steppe to seasonal variations in soil moisture. Journal of Geophysical Research 113 (G1).
Liu, S., Mao, D., Lu, L., 2006. Measurement and estimation of the aerodynamic resistance. Hydrology and Earth System Sciences Discussions 3 (3), 681–705.
Liu, J., Gao, J., Lv, S., Han, Y., Nie, Y., 2011. Shifting farming–pastoral ecotone in China under climate and land use changes. Journal of Arid Environments 75 (3), 298–308.
Lu, Y., Zhuang, Q., Zhou, G., Sirin, A., Melillo, J., Kicklighter, D., 2009. Possible decline of the carbon sink in the Mongolian Plateau during the 21st century. Environmental Research Letters 4 (4), 045023.
Lu, N., Chen, S., Wilske, B., Sun, G., Chen, J., 2011. Evapotranspiration and soil water relationships in a range of disturbed and undisturbed ecosystems in the semi-arid Inner Mongolia, China. Journal of Plant Ecology 4, 49–60.
L'vovich, M.I., White, G.F., Belyaev, A.V., Kindler, J., Koronkevic, N.I., Lee, T.R., Voropaev, G.V., 1990. Use and transformation of terrestrial water systems. The earth as transformed by human action. Cambridge University Press, Cambridge, UK, pp. 235–252.
Massmana, W.J., Lee, X., 2002. Eddy covariance flux corrections and uncertainties in long-term studies of carbon and energy exchanges. Agricultural and Forest Meteorology 113, 121–144.
McGuire, A.D., Melillo, J.M., Joyce, L.A., Kicklighter, D.W., Grace, A.L., Moore III, B., Vorosmarty, C.J., 1992. Interactions between carbon and nitrogen dynamics in estimating net primary productivity for potential vegetation in North America. Global Biogeochemical Cycles 6, 101–124.
McGuire, A.D., Melillo, J.M., Kicklighter, D.W., Pan, Y., Xiao, X., Helfrich, J., Moore, B., Vorosmarty, C.J., Schloss, A.L., 1997. Equilibrium responses of global net primary production and carbon storage to doubled atmospheric carbon dioxide: sensitivity to changes in vegetation nitrogen concentration. Global Biogeochemical Cycles 11 (2), 173–189.
Miglietta, F., Peressotti, A., Viola, R., Körner, C., Amthor, J.S., 2011. Stomatal numbers, leaf and canopy conductance, and the control of transpiration. Proceedings of the National Academy of Sciences 108 (28), E275-E275.
Milner, K.S., Coble, D.W., McMahan, A.J., Smith, E.L., 2003. FVSBGC: a hybrid of the physiological model STAND-BGC and the forest vegetation simulator. Canadian Journal of Forest Research 33 (3), 466–479.
Miralles, D.G., Gash, J.H., Holmes, T.R., de Jeu, R.A., Dolman, A.J., 2010. Global canopy interception from satellite observations. Journal of Geophysical Research-Atmospheres (1984–2012) 115 (D16).
Miralles, D.G., De Jeu, R.A.M., Gash, J.H., Holmes, T.R.H., Dolman, A.J., 2011a. Magnitude and variability of land evaporation and its components at the global scale. Hydrology and Earth System Sciences 15 (3), 967–981.
Miralles, D.G., Holmes, T.R.H., De Jeu, R., Gash, J.H., Meesters, A.G.C.A., Dolman, A.J., 2011b. Global land-surface evaporation estimated from satellite-based observations. Hydrology and Earth System Sciences 15 (2), 453–469.
Mitchell, T.D., Jones, P.D., 2005. An improved method of constructing a database of monthly climate observations and associated high-resolution grids. International Journal of Climatology 25 (6), 693–712.
Monteith, J.L., 1965. Evaporation and environment. Symposium of the society of experimental biology 19, 205–224.
Moore, C.J., 1986. Frequency response corrections for eddy correlation systems. Boundary-Layer Meteorology 37, 17–35.
Mu, Q., Heinsch, F.A., Zhao, M., Running, S.W., 2007. Development of a global evapotranspiration algorithm based on MODIS and global meteorology data. Remote Sensing of Environment 111 (4), 519–536.
Mu, Q., Zhao, M., Running, S.W., 2011. Improvements to a MODIS global terrestrial evapotranspiration algorithm. Remote Sensing of Environment 115 (8), 1781–1800.
Mueller, B., et al., 2011. Evaluation of global observations-based evapotranspiration datasets and IPCC AR4 simulations. Geophysical Research Letters 38 (6), L06402.
New, M., Hulme, M., Jones, P., 1999. Representing twentieth-century space-time climate variability. Part I: development of a 1961–90 mean monthly terrestrial climatology. Journal of Climate 12 (3), 829–856.
New, M., Hulme, M., Jones, P., 2000. Representing twentieth-century space–time climate variability. Part II: development of 1901–96 monthly grids of terrestrial surface climate. Journal of Climate 13 (13), 2217–2238.
Oki, T., Kanae, S., 2006. Global hydrological cycles and world water resources. Science 313 (5790), 1068–1072.
Pan, Y., Mcguire, A.D., Kicklighter, D.W., Melillo, J.M., 1996. The importance of climate and soils for estimates of net primary production: a sensitivity analysis with the terrestrial ecosystem model. Global Change Biology 2 (1), 5–23.
Papale, D., Valentini, R., 2003. A new assessment of European forests carbon exchanges by eddy fluxes and artificial neural network spatialization. Global Change Biology 9 (4), 525–535.

Peterson, B.J., et al., 2002. Increasing river discharge to the Arctic Ocean. Science 298 (5601), 2171–2173.
Peterson, B.J., et al., 2006. Trajectory shifts in the Arctic and subarctic freshwater cycle. Science 313 (5790), 1061–1066.
Pierce, L.L., Running, S.W., Walker, J., 1994. Regional-scale relationships of leaf area index to specific leaf area and leaf nitrogen content. Ecological Applications 4 (2), 313–321.
Poorter, H., Evans, J.R., 1998. Photosynthetic nitrogen-use efficiency of species that differ inherently in specific leaf area. Oecologia 116 (1), 26–37.
Raich, J.W., Rastetter, E.B., Melillo, J.M., Kicklighter, D.W., Steudler, P.A., Peterson, B.J., Grace, A.L., Moore III, B., Vorosmarty, C.J., 1991. Potential net primary productivity in South America: application of a global model. Ecological Applications 1 (4), 399–429.
Running, S.W., Coughlan, J.C., 1988. A general model of forest ecosystem processes for regional applications I. Hydrologic balance, canopy gas exchange and primary production processes. Ecological Modelling 42 (2), 125–154.
Salomon, J., Schaaf, C.B., Strahler, A.H., Gao, F., Jin, Y., 2006. Validation of the MODIS bidirectional reflectance distribution function and albedo retrievals using combined observations from the aqua and terra platforms. IEEE Transactions on Geoscience and Remote Sensing 44 (6), 1555–1565.
Sankey, T.T., Montagne, C., Graumlich, L., Lawrence, R., Nielsen, J., 2006. Lower forest–grassland ecotones and 20th century livestock herbivory effects in northern Mongolia. Forest Ecology and Management 233 (1), 36–44.
Schaaf, C.B., Gao, F., Strahler, A.H., Lucht, W., Li, X., Tsang, T., Strugnell, N.C., Zhang, X., Jin, Y., Muller, J.P., 2002. First operational BRDF, albedo nadir reflectance products from MODIS. Remote Sensing of Environment 83 (1–2), 135–148.
Schmid, H.P., 1994. Source areas for scalars and scalar fluxes. Boundary-Layer Meteorology 67 (3), 293–318.
Schmid, H.P., 1997. Experimental design for flux measurements: matching scales of observations and fluxes. Agricultural and Forest Meteorology 87 (2), 179–200.
Schmid, H.P., Lloyd, C.R., 1999. Spatial representativeness and the location bias of flux footprints over inhomogeneous areas. Agricultural and Forest Meteorology 93 (3), 195–209.
Scott, R.L., 2010. Using watershed water balance to evaluate the accuracy of eddy covariance evaporation measurements for three semiarid ecosystems. Agricultural and Forest Meteorology 150 (2), 219–225.
Sellers, P.J., Mintz, Y., Sud, Y.C., Dalcher, A., 1986. A simple biosphere model (SiB) for use within general circulation models. Journal of the Atmospheric Sciences 43 (6), 505–531.
Serreze, M.C., Barry, R.G., 2005. The Arctic Climate System. Cambridge University Press, Cambridge.
Shiklomanov, I., Sokolov, A., Beken, A., Herrmann, A., 1983. Methodological basis of world water balance investigation and computation. IAHS Publication 148, 77–92.
Shukla, J., Nobre, C., Sellers, P., 1990. Amazon deforestation and climate change. Science (Washington) 247 (4948), 1322–1325.
Shuttleworth, W.J., 1992. Evaporation. In: Maidment, D.R. (Ed.), Handbook of Hydrology. McGraw Hill, New York, pp. 4.1–4.53.
Sokolov, A.P., Schlosser, C.A., Dutkiewicz, S., Paltsev, S., Kicklighter, D.W., Jacoby, H.D., Prinn, R.G., Forest, C.E., Reilly, J.M., Wang, C., 2005. MIT integrated global system model(IGSM) version 2: model description and baseline evaluation. MIT Joint Program on the Science and Policy of Global Change Report. Report, 124. MIT Joint Program on the Science and Policy of Global Change, Cambridge, Massachusetts.
Sprintsin, M., Karnieli, A., Berliner, P., Rotenberg, E., Yakir, D., Cohen, S., 2009. Evaluating the performance of the MODIS Leaf Area Index (LAI) product over a Mediterranean dryland planted forest. International Journal of Remote Sensing 30 (19), 5061–5069.
Strahler, A.H., Friedl, M., Zhang, X., Hodges, J., Cooper, C.S.A., Baccini, A., 2002. The MODIS land cover and land cover dynamics products. Presentation at Remote Sensing of the. Earth's. Environment from Terra in L'Aquila, Italy.
Sun, W., Wu, W., Zhang, B., 2002. An approach to the fluctuation mechanism of ecotone. Journal of Environmental Sciences 14 (1), 127–131.
Sun, G., Alstad, K., Chen, J., Chen, S., Ford, C.R., Lin, G., Liu, C., Lu, N., McNulty, S.G., Miao, H., 2011a. A general predictive model for estimating monthly ecosystem evapotranspiration. Ecohydrology 4 (2), 245–255.
Sun, G., Caldwell, P., Noormets, A., McNulty, S.G., Cohen, E., Moore Myers, J., Domec, J.C., Treasure, E., Mu, Q., Xiao, J., 2011b. Upscaling key ecosystem functions across the conterminous United States by a water-centric ecosystem model. Journal of Geophysical Research – Biogeosciences 116 (G3).
Tchebakova, N.M., Kolle, O., Zolotoukhine, D., Arneth, A., Styles, J.M., Vygodskaya, N.N., Schulze, E., Shibistova, O., Lloyd, J., 2002. Inter-annual and seasonal variations of energy and water vapour fluxes above a Pinus sylvestris forest in the Siberian middle taiga. Tellus B 54 (5), 537–551.
Tchebakova, N.M., Parfenova, E., Soja, A.J., 2009. The effects of climate, permafrost and fire on vegetation change in Siberia in a changing climate. Environmental Research Letters 4 (4), 045013.
Tchebakova, N.M., Parfenova, E.I., Soja, A.J., 2011. Climate change and climate-induced hot spots in forest shifts in central Siberia from observed data. Regional Environmental Change 11 (4), 817–827.
Turner, D.P., Ritts, W.D., Cohen, W.B., Gower, S.T., Zhao, M., Running, S.W., Wofsy, S.C., Urbanski, S., Dunn, A.L., Munger, J.W., 2003. Scaling Gross Primary Production (GPP) over boreal and deciduous forest landscapes in support of MODIS GPP product validation. Remote Sensing of Environment 88 (3), 256–270.
Valiantzas, J.D., 2006. Simplified versions for the Penman evaporation equation using routine weather data. Journal of Hydrology 331 (3–4), 690–702.
Vinukollu, R.K., Wood, E.F., Ferguson, C.R., Fisher, J.B., 2011. Global estimates of evapotranspiration for climate studies using multi-sensor remote sensing data: evaluation of three process-based approaches. Remote Sensing of Environment 115 (3), 801–823.
Vörösmarty, C.J., Federer, C.A., Schloss, A.L., 1998. Potential evaporation functions compared on U.S. watersheds: possible implications for global-scale water balance and terrestrial ecosystem modeling. Journal of Hydrology 207 (3–4), 147–169.
Vorosmarty, C.J., Green, P., Salisbury, J., Lammers, R.B., 2000. Global water resources: vulnerability from climate change and population growth. Science 289 (5477), 284–288.
Wang, K., Dickinson, R.E., 2012. A review of global terrestrial evapotranspiration: observation, modeling, climatology, and climatic variability. Reviews of Geophysics 50 (2).
Wang, Y., Woodcock, C.E., Buermann, W., Stenberg, P., Voipio, P., Smolander, H., Häme, T., Tian, Y., Hu, J., Knyazikhin, Y., Myneni, R.B., 2004. Evaluation of the MODIS LAI algorithm at a coniferous forest site in Finland. Remote Sensing of Environment 91 (1), 114–127.
Wang, Q., Tenhunen, J., Dinh, N.Q., Reichstein, M., Otieno, D., Granier, A., Pilegarrd, K., 2005. Evaluation of seasonal variation of MODIS derived leaf area index at two European deciduous broadleaf forest sites. Remote Sensing of Environment 96 (3), 475–484.
Wang, K., Dickinson, R.E., Wild, M., Liang, S., 2010. Evidence for decadal variation in global terrestrial evapotranspiration between 1982 and 2002: 1. Model development. Journal of Geophysical Research 115 (D20), D20112.
Wang, Y., Yu, P., Feger, K.H., Wei, X., Sun, G., Bonell, M., Xiong, W., Zhang, S., Xu, L., 2011. Annual runoff and evapotranspiration of forestlands and non-forestlands in selected basins of the Loess Plateau of China. Ecohydrology 4 (2), 277–287.
Webster, M.D., et al., 2002. Uncertainty in emissions projections for climate models. Atmospheric Environment 36 (22), 3659–3670.
Weiß, M., Menzel, L., 2008. A global comparison of four potential evapotranspiration equations and their relevance to stream flow modelling in semi-arid environments. Advances in Geosciences 18, 15–23.
White, M.A., Thornton, P.E., Running, S.W., Nemani, R.R., 2000. Parameterization and sensitivity analysis of the BIOME-BGC terrestrial ecosystem model: net primary production controls. Earth Interactions 4 (3), 1–85.
Wilson, K., Goldstein, A., Falge, E., Aubinet, M., Baldocchi, D., Berbigier, P., Bernhofer, C., Ceulemans, R., Dolman, H., Field, C., 2002. Energy balance closure at FLUXNET sites. Agricultural and Forest Meteorology 113 (1), 223–243.
Wright, I.R., Manzi, A.O., Da Rocha, H.R., 1995. Surface conductance of Amazonian pasture: model application and calibration for canopy climate. Agricultural and Forest Meteorology 75 (1), 51–70.
Xiao, J., Chen, J., Davis, K.J., Reichstein, M., 2012. Advances in upscaling of eddy covariance measurements of carbon and water fluxes. Journal of Geophysical Research 117, G00J01.
Xu, L., Dennis, P.L., Wood, E.F., Burges, S.J., 1994. A simple hydrologically based model of land surface water and energy fluxes for general circulation models. Journal of Geophysical Research 99, 14415–14428.
Yang, W., Tan, B., Huang, D., Rautiainen, M., Shabanov, N.V., Wang, Y., Privette, J.L., Huemmrich, K.F., Fensholt, R., Sandholt, I., 2006. MODIS leaf area index products: from validation to algorithm improvement. IEEE Transactions on Geoscience and Remote Sensing 44 (7), 1885–1898.
Zhang, Y., Kadota, T., Ohata, T., Oyunbaatar, D., 2007. Environmental controls on evapotranspiration from sparse grassland in Mongolia. Hydrological Processes 21 (15), 2016–2027.
Zhao, M., Running, S.W., Nemani, R.R., 2006. Sensitivity of Moderate Resolution Imaging Spectroradiometer (MODIS) terrestrial primary production to the accuracy of meteorological reanalyses. Journal of Geophysical Research 111 (G1), G01002.
Zhu, X., Zhuang, Q., Chen, M., Sirin, A., Melillo, J., Kicklighter, D., Sokolov, A., Song, L., 2011. Rising methane emissions in response to climate change in Northern Eurasia during the 21st century. Environmental Research Letters 6 (4), 045211.
Zhuang, Q., Romanovsky, V.E., McGuire, A.D., 2001. Incorporation of a permafrost model into a large-scale ecosystem model: evaluation of temporal and spatial scaling issues in simulating soil thermal dynamics. Journal of Geophysical Research 106 (D24), 33,649–33,670.
Zhuang, Q., McGuire, A.D., O'Neill, K.P., Harden, J.W., Romanovsky, V.E., Yarie, J., 2002. Modeling soil thermal and carbon dynamics of a fire chronosequence in interior Alaska. Journal of Geophysical Research 108 (D1).
Zhuang, Q., McGuire, A.D., Melillo, J.M., Clein, J.S., Dargaville, R.J., Kicklighter, D.W., Myneni, R.B., Dong, J., Romanovsky, V.E., Harden, J., Hobbie, J.E., 2003. Carbon cycling in extratropical terrestrial ecosystems of the Northern Hemisphere during the 20th Century: a modeling analysis of the influences of soil thermal dynamics. Tellus 55B, 751–776.
Zhuang, Q., Melillo, J.M., Kicklighter, D.W., Prinn, R.G., McGuire, D.A., Steudler, P.A., Felzer, B.S., Hu, S., 2004. Methane fluxes between terrestrial ecosystems and the atmosphere at northern high latitudes during the past century: a retrospective analysis with a process-based biogeochemistry model. Global Biogeochemical Cycles 18 (3).
Zhuang, Q., et al., 2010. Carbon dynamics of terrestrial ecosystems on the Tibetan Plateau during the 20th century: an analysis with a process-based biogeochemical model. Global Ecology and Biogeography 19 (5), 649–662.
Zobler, L., 1986. A world soil file for global climate modeling. NASA Technical Memorandum 87802. National Aeronautics and Space Administration, New York.